To the Graduate Council:

I am submitting herewith a thesis written by Hojung Sin entitled "A Polyphase Power Supply and Peristaltic Flow Accelerator Using a One Atmosphere Uniform Glow Discharge Plasma (OAUGDP^{TM})." I have examined the final paper copy of this thesis for form and content and recommend that it be accepted in partial fulfillment of requirements for the degree of Master of Science, with a major in Electrical Engineering.

J. Reece Roth, Major Professor

We have read this thesis and recommend its acceptance:

Acceptance for the Council:

Vice Provost and Dean of Graduate Studies

A POLYPHASE POWER SUPPLY AND PERISTALTIC FLOW ACCELERATOR USING A ONE ATMOSPHERE UNIFORM GLOW DISCHARGE PLASMA (OAUGDP^{TM})

A Thesis
Presented for the
Master of Science
Degree

The University of Tennessee, Knoxville

Hojung Sin
December 2002

DEDICATION

This thesis is dedicated to my parents
Mr. Bongki Shin and Mrs. Soonam Lee.

who gave me my life on earth.

ACKNOWLEDGEMENTS

There are many people to whom I am thankful for contributing to my educational experience at the University of Tennessee. I would like to thank Professor J. Reece Roth, for his financial support, the opportunity to do research, and for assistance in editing the manuscript. I would also like to thank my dissertation committee, Professor Marshall O. Pace, and Professor M. Mostofa Howlader for their encouragement. I would also like to express my appreciation to Mr. Stephen P. Wilkinson of the NASA Langley Research Center for his helpful comments and assistance while I worked there.

My research was supported by AFOSR contract AF F49620-01-1-0425, Dr. John Schmisseur, program manager.

ABSTRACT

A surface layer of One Atmosphere Uniform Glow Discharge Plasma (OAUGDP^{TM}) was generated by parallel strip electrodes on a flat panel using a polyphase power supply system. Each electrode is energized by one of eight phases, and the phase of each electrode is increased or decreased with respect to its neighbors by a phase angle controlled by a LabView DAQ device. The phase angle between adjacent electrodes was normally 45°, the operating frequency was in the range from 0.5 kHz to 6 kHz, and the maximum output voltage was 6-7 kVrms. The DAQ device was designed to generate up to 8 channels of analog output. The polyphase power supply system was engineered to eliminate RFI and instabilities, and to maintain a steady state voltage output on each phase. Various methods using high voltage diodes were introduced for DC and AC operation to improve the stability of the power supply system.

Peristaltic acceleration of the neutral gas above the panel was demonstrated. One may go to the website http://plasma.ece.utk.edu/ and click on the video clips to see a demonstration of peristaltic flow acceleration. The general features of the peristaltically-induced flow were consistent with theoretical predictions. Digital images of the peristaltic flow show that there exist unsteady flow regions that may reduce the peristaltic velocity. The peristaltically-induced neutral gas velocity in these early, low voltage experiments was measured to be 3-6 m/sec.

TABLE OF CONTENTS

LIST OF FIGURES

1. INTRODUCTION

Plasma exists in our everyday life from tiny discharges of static electricity to huge lightening bolts, and more than ninety-five percent of the known matter in the universe is in the plasma state [11, 12]. The term "plasma", first introduced by Irving Langmuir in 1926, means a collection of ions and electrons that is approximately electrically neutral [11]. In our everyday life, the concept and reality of the plasma state of matter are familiar, although most people cannot say what it is. If the plasma state of matter can contribute to the next generation of our transportation systems, its scientific study and engineering development will be amply justified on these grounds alone.

The characteristics of the plasma state at one atmosphere have not been easy to diagnose since high electron collision frequencies and electron collision mean free paths shorter than the Debye length produce questionable data from standard Langmuir probes and microwave interferometers [11, 16, 17]. Research and development of glow discharge plasmas has been done in vacuum systems over the last 200 years. However, in recent developments at the UT Plasma Sciences Laboratory, a One Atmosphere Uniform Glow Discharge Plasma (OAUGDP™) has been generated at atmospheric pressure in air rather than in vacuum systems, using low frequency RF excitation [1, 6, 13, 15, 19].

The OAUGDP™ developed at the University of Tennessee Plasma Sciences Laboratory has been used for increasing the surface energy and sterilization of surfaces [17, 19]. These applications are being commercialized by a local spin-off company, Atmospheric Glow Technologies, Inc. One may visit the company's home page, http://www.a-gtech.com/.

A potential application of the OAUGDP™ is in aviation to improve aircraft control systems [3, 8, 14, 20, 21]. Current control systems utilize rudders, flaps, and ailerons actuated by complex mechanical and hydraulic systems. To prevent the formation of vortices, to promote attached steady-state air flow over the airfoils, to reduce drag, and to add momentum to the flow for directional control, the surface of an aircraft can be energized by an OAUGDP™. To achieve this new application, one can create an OAUGDP™ on the aerodynamically active surface that does not interfere with the air flow, but increases its speed and stability [14, 21].

Walsh and Kimura have investigated another approach using a Micro Electro-Mechanical (MEM) system [7, 24]. However, it is not practical to attach micro-size motor systems on the surface of an aircraft wing because of its exposure to air, its speed generation limitations, maintainability issues, and technical problems with its power supply system.

The plasma method is a simpler way to modify the airflow than the Micro Electro-Mechanical (MEM) system. To generate an OAUGDP™, one can attach a series of insulated metal electrodes on the surface of an aircraft, and only a simple power supply system is required. Such OAUGDP™ panels are mechanically robust, and their maintenance and operation is simple compared to the Micro Electro-Mechanical (MEM) system.

To utilize the one atmospheric glow discharge plasma (OAUGDP™) for aerodynamic applications, Roth formulated a theory based on momentum transfer to the surrounding air by Lorentzian collisions [17]. The theory is based on the ion trapping mechanism for generating the OAUGDP™, paraelectric effects, ion mobility momentum transfer, and peristaltic effects [17]. Its mechanisms are reviewed in the next chapter.

Most of this paper is devoted to the initial peristaltic flow experiments, based on accelerating the ions and neutral gas flow by a traveling electrostatic wave. To create the peristaltic motion, one needs a multiple-channel power supply system to generate polyphase high RF voltages. The design and construction of a polyphase power supply system capable of up to 7 kVrms at frequencies from 0.5 to 10 kHz are the subject of this thesis. A characteristic experimental set-up is shown in Figure 1.1.

The data relating to peristaltically-induced flow velocities and the video of a peristaltic smoke flow demonstration (http://plasma.ece.utk.edu/, video clips) were taken on the 7 x 11 Low Speed Wind Tunnel at the NASA Langley Research Center in Hampton, VA with the assistance of Mr. Stephen P. Wilkinson. A crude flow demonstration around a cylinder, available for viewing at the above website, was based on research at the UT Plasma Sciences Laboratory.

Most of the contributions of this thesis focus on the multi-channel polyphase high voltage power supply system as the key requirement to energize the plasma for peristaltic flow acceleration. The goal is to generate a maximum output of 7-8 kV_{rms} on each electrode without tracking or arcing problems. Our test panels typically consist of three RF periods, each period with eight electrodes, one for each phase. The voltage on individual electrodes is easily affected by RFI in the form of voltage spikes that propagate through system. Methods to deal with Radio Frequency Interference (RFI), and to prevent arcing and tracking problems are discussed.

The author hopes this work will help those who want to design and construct not only a peristaltic plasma polyphase power supply system, but also a single phase or DC operating power supply system as well.

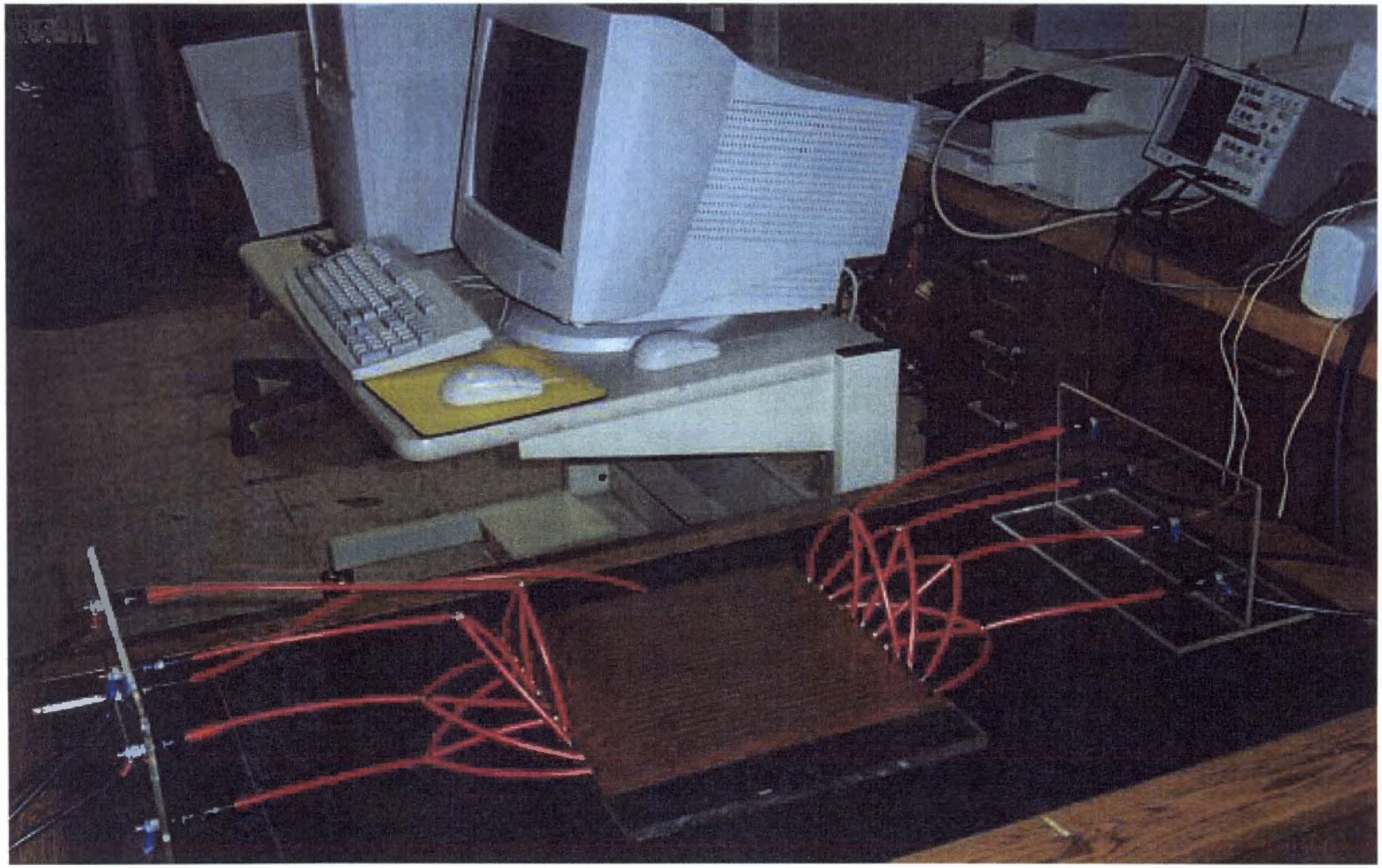

Figure 1.1 Peristaltic flow acceleration experiment at the UT Plasma Sciences Laboratory. The peristaltic 3-period panel and control system are shown. A video clip showing peristaltic acceleration of neutral gas flow above this panel is available at the UT Plasma Science Laboratory website, http://plasma.ee.utk.edu

2. TWO SUBDISCIPLINES OF PLASMA PHYSICS

2.1 Magnetohydrodynamics (MHD)

Magnetohydrodynamics is concerned with the behavior of electrically conducting fluids in magnetic fields. Magnetohydrodynamic (MHD) methods were investigated for aerodynamic flow control applications previous to electrohydrodnamic (EHD) methods [23]. The use of MHD for turbulent viscous drag reduction is based on coupling momentum to the flow by the magnetic body force

$$\mathbf{F} = \mathbf{J} \times \mathbf{B}, \quad (1)$$

where

$$\mathbf{J} = e n_e \mathbf{v}, \quad (2)$$

v is the drift velocity of a positive charge, n_e is the electron number density, **B** is the magnetic induction, and **J** is the current density in the plasma. The momentum transfer to the plasma by the magnetic body force can be increased by applying high currents in the plasma and strong magnetic fields. MHD methods require robust electrodes that can resist the current, and powerful magnets to generate high magnetic fields. The MHD approach is undesirable for real aerodynamic applications since its current source, magnetic field coils, and electrodes are not easily attached to an aircraft wing.

2.2 Electrohydrodynamics (EHD)

Electrohydrodynamics (EHD) is the behavior of electrically charged fluids in electric fields. EHD flow control for aerodynamics has received less attention than MHD approaches because the generation of atmospheric glow discharge plasmas by electric fields alone was not believed to be possible. However, the group at the University of Tennessee Plasma Sciences Laboratory successfully developed the One Atmosphere Uniform Glow Discharge Plasma (OAUGDP^{TM}) with electric fields alone. The advantages of EHD over MHD is its simple, robust electrode structure, no need for magnetic fields, and steady state operation. Industrial applications involving EHD principles include electrostatic paint spraying, electrostatic precipitators, and electrodeposition.

2.2.1 Characteristics of the OAUGDP^{TM} as an EHD Device

The One Atmosphere Uniform Glow Discharge Plasma (OAUGDP^{TM}) requires only electric fields. It does not require magnetic fields or a low pressure vacuum system. The OAUGDP^{TM} is generated by a low frequency RF power supply instead of DC voltages. Displacement currents are used to generate OAUGDP^{TM} plasma, and real currents are not required. The frequency used to generate the OAUGDP^{TM} is normally lower than 10 kHz.

The essential feature of the OAUGDP^{TM} is the ion trapping mechanism. This mechanism is a constrained and periodic oscillation of ions along electric fields lines. The RF voltage drives an oscillation of ions with the applied frequency between the electrodes of the OAUGDP^{TM}, such that the ions transit the gap between electrodes, but do not reach the electrodes during a half-cycle of the RF. The term *ion trapping*, and its physical mechanism were described by J. R. Roth, in his book, *Industrial Plasma Engineering,* Vol.1., Section 12.5.2 [17]. The driving frequency necessary to achieve ion trapping is,

$$\nu_o = \frac{ZV_{rms}e}{\pi M d^2 \nu_c} \quad (3)$$

where ν_o is the RF frequency required to trap ions, Z is the charge on the ions, V_{rms} is the driving rms voltage, M is the ion mass, d is the gap distance between electrodes, and ν_c is the ion-neutral collision frequency.

The OAUGDP™ is a non-equilibrium plasma. Unlike DC glow discharges at low pressure, the electron kinetic temperature, electron number density, and ion number density are time dependent and vary with the RF voltage cycle. The energy cost of generating OAUGDP™ is low because, as a glow discharge, it operates at the Stoletow point [11], where the energy cost of generating an ion-electron pair is a minimum, 81eV for air. The device is light due to the absence of magnets and large dissipative currents. Thus, it can be used in flight boundary layer flow control or drag reduction applications.

2.2.2 The Paraelectric Body Force

Paraelectric effects are the electrostatic analog of paramagnetism, and result from an electrostatic body force that acts on the net charge density of a plasma to accelerate it in the direction of an increasing electric field gradient. These effects refer to the ability of a non-uniform electric field to exert a unidirectional force on a electrically neutral but polarized dielectric. The resulting neutral gas flow velocity at one atmosphere is on the order of one to ten meters per second, and the resultant force is in the direction of an increasing electric field gradient.

The flow of neutral gas that results from paraelectric effects can be understood in terms of the Lorentzian formalism in which each collision of an ion or electron gives up to the neutral background gas all the momentum acquired from the electric field since the last collision. The magnitude and direction of the induced acceleration of the surrounding neutral gas are determined by the Lorentzian momentum transfer. As illustrated in Figure 2.1, the plasma moves from low to high electric field gradient, and drags the neutral gas along with it as a result of ion-neutral collisions.

To formulate a theory of the paraelectric EHD body force, the electrostatic body force is introduced [17].

$$F_E = \rho_c E \qquad \text{newtons/m}^3 \tag{4}$$

where ρ_c is the net charge density,

$$\rho_c = e(Zn_i - n_e) \qquad \text{coulombs/m}^3 \tag{5}$$

Z is the state of ionization, n_i is the ionic number density, and n_e is the electron number density.

Posisson's equation can be introduced to calculate the electrostatic body force,

$$\nabla \cdot E = \frac{\rho_c}{\varepsilon_o} \tag{6}$$

where ε_o is the dielectric constant. By substituting equation (6) into equation (4), the body force is given as,

$$F_E = \varepsilon_o E \nabla \cdot E = \frac{d}{dx}\left(\frac{1}{2}\varepsilon_o E^2\right) \qquad \text{newtons/m}^3 \tag{7}$$

The term in the parentheses can be expressed as the electrostatic pressure, p_E, having the units of newtons per square meter.

The gradients of ideal gas law pressure and electrostatic pressure will be approximately in equilibrium if no external forces act,

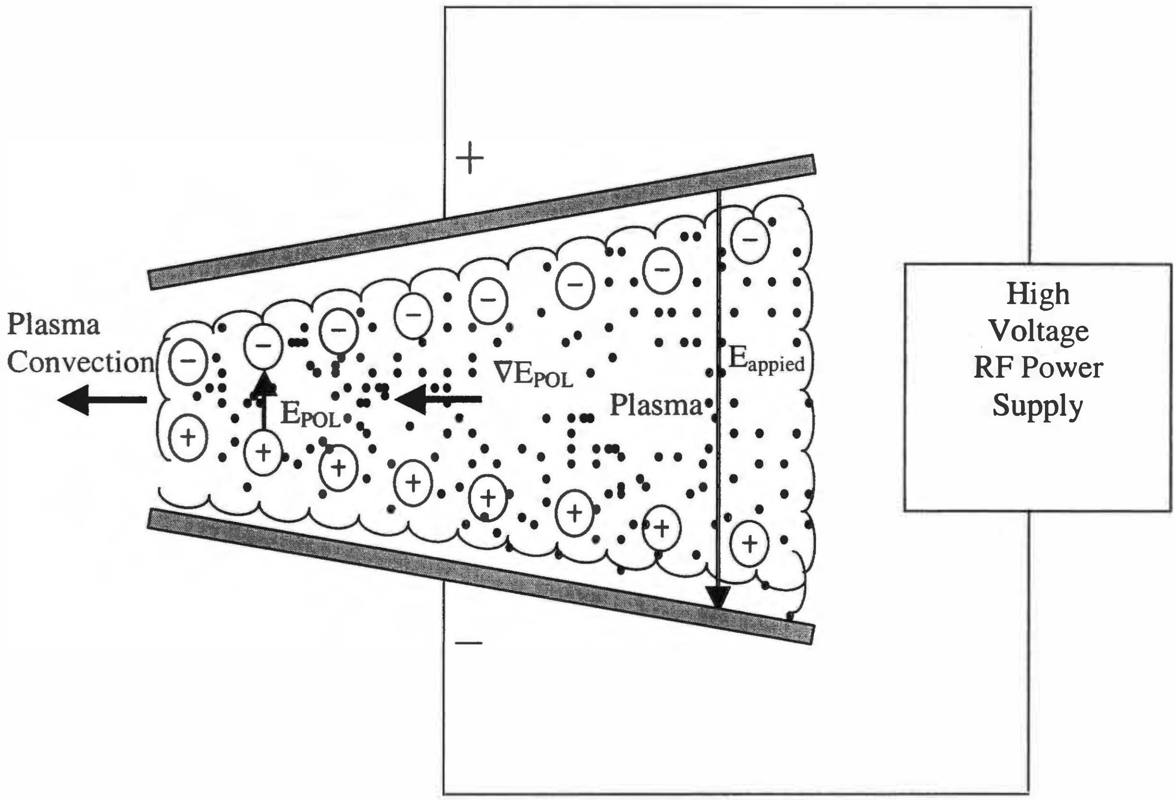

Figure 2.1 Paraelectric polarized plasma between two tilted electrodes. Plasma motion is to the left

$$\nabla p_g + \nabla p_E = \frac{d}{dx}(p_g + p_E) = 0, \qquad (8)$$

where p_g is the ideal gasdynamic pressure, nkT.

Substituting p_E and p_g and solving equation (8), one obtains

$$nkT + \frac{\varepsilon_o}{2} E^2 = \text{constant}. \qquad (9)$$

From equation (9), one can understand that the neutral gas pressure in the plasma, p_g, is smaller than the surrounding regions without electric fields. This causes an inflow of the surrounding higher pressure gas. The term "paraelectric effects", implies that the plasma ions and the neutral gas are coupled, so that the ions can transfer their momentum to the neutral molecules, and accelerate neutral gas away from a region of high electric field gradients.

If the neutral gas flowing away from the plasma has a velocity v_o, the dynamic (or stagnation) pressure will be equal to the electrostatic pressure,

$$p_s = \frac{1}{2}\rho {v_o}^2 = \frac{1}{2}\varepsilon_o E^2 \qquad \text{newtons/m}^2; \qquad (10)$$

where p_s is the stagnation pressure, and v_o is the neutral gas velocity.

The induced neutral gas flow velocity v_o can be obtained

$$v_o = E\sqrt{\frac{\varepsilon_o}{\rho}} \qquad \text{meters/sec}, \qquad (11)$$

which is a function of the mass density of the working gas (1.3 kg/m^3 for air at one atmosphere) and the electric field.

2.2.3 Ion Mobility Drift

The next EHD flow acceleration mechanism is *ion mobility drift* [17]. Ions or electrons can drift in horizontal DC electric fields along the surface of a flat panel consisting of strip electrodes, as shown in Figure 2.2. A horizontal electric field is maintained between electrodes by a DC power supply and a resistor string. These electric fields will cause ions and electrons to drift in opposite directions. The ion drift velocity dominates the momentum transfer to the neutral gas as a result of Lorentzian collisions.

The loss of momentum by electrons and their volumetric Lorentzian momentum loss can be formulated as,

$$\dot{M}_e = mn_e v_{de} \nu_{en} \qquad \text{kg-m/sec}^2\text{-m}^3, \qquad (12)$$

where v_{de} is the electron drift velocity, m is the electron mass, and the electron collision frequency is given by

$$\nu_{en} = n_o \langle \sigma v \rangle_{en} \qquad \text{electron collisions/sec.} \qquad (13)$$

Substituting equation (13) into equation (12), the result is,

$$\dot{M}_e = mv_{de} n_o n_e \langle \sigma v \rangle_{en} = mv_{de} R_{en} \qquad \text{kg-m/sec}^2\text{-m}^3 \qquad (14)$$

where reaction rate, R_{en} is the total number of electron-neutral collisions per second and per cubic meter.

The volumetric momentum received by the neutral gas from the electrons is given by,

$$\dot{M}_o = M_o n_o v_{oe} \nu_{ne} = M_o v_{oe} R_{ne} \qquad \text{kg-m/sec}^2\text{-m}^3 \qquad (15)$$

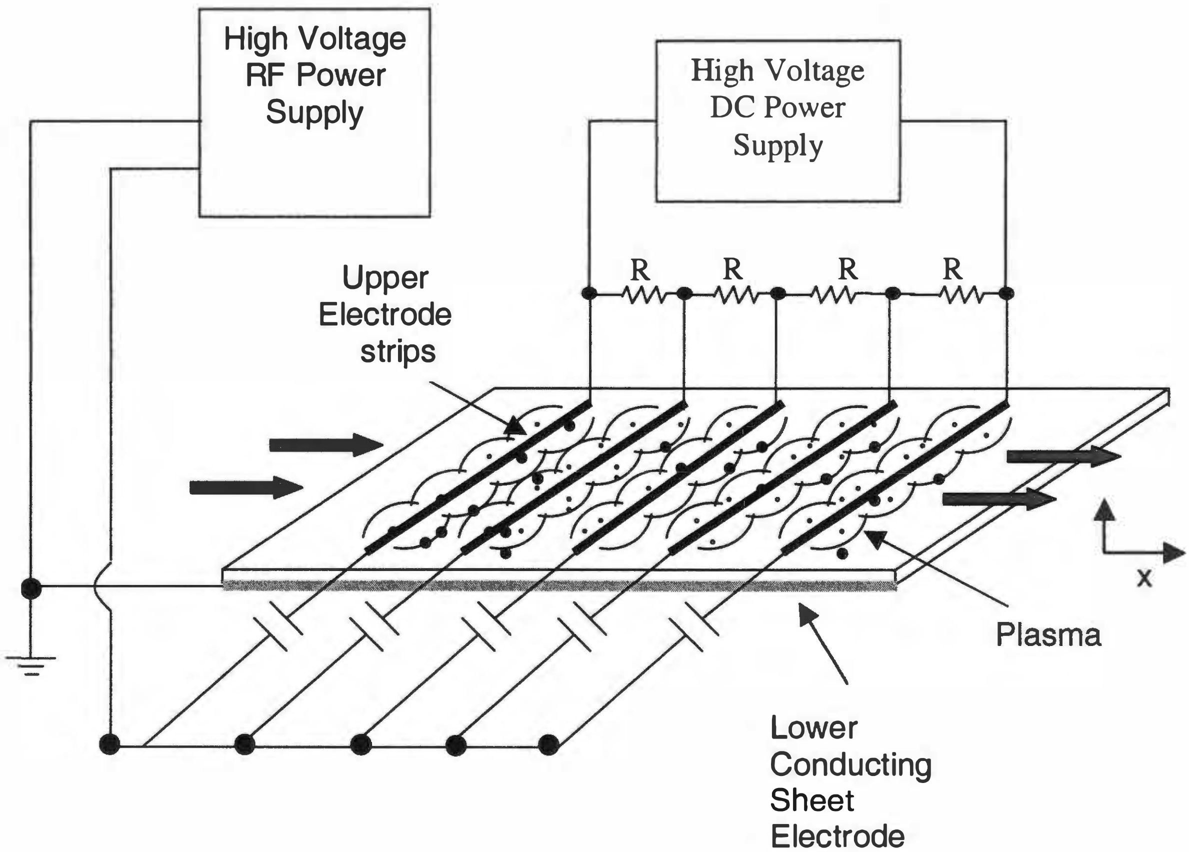

Figure 2.2 DC plasma accelerator panel with strip electrodes. The electrodes are driven by a single phase RF power supply, while a horizontal electric field is maintained by a resistor string and a DC power supply.

where M_o is the neutral mass, 28.5 proton masses for air, and the neutral collision frequency with electrons is given by,

$$\nu_{ne} = n_e \langle \sigma v \rangle_{ne} \qquad \text{neutral collisions/sec} \qquad (16)$$

One can combine equation (15) and equation (16), and the result is,

$$\dot{M}_o = M_o v_{oe} n_o n_e \langle \sigma v \rangle_{ne} = M v_{oe} R_{ne} \qquad \text{kg-m/sec}^2\text{-m}^3 \qquad (17)$$

where v_{oe} is the electron drift-induced neutral convection velocity. Since equation (17) and equation (14) should be same, and $R_{ne} = R_{en}$ as a result of the binary nature of the collisions, one can derive the result

$$M_o v_{oe} n_o n_e \langle \sigma v \rangle_{ne} = m v_{de} n_o n_e \langle \sigma v \rangle_{en} \qquad (18)$$

Solving for the neutral gas drift velocity induced by electron collisions, one obtains

$$v_{oe} = \frac{m v_{de}}{M_o} \qquad \text{meter/sec} \qquad (19)$$

Since the electron mobility drift velocity can be expressed by,

$$v_{de} = \mu_e E = \frac{eE}{m\nu_{en}} \qquad \text{meters/sec} \qquad (20)$$

the equation (18b) becomes,

$$v_{oe} = \frac{eE}{M_o \nu_{en}} \qquad \text{meters/sec} \qquad (21)$$

In a similar way, one can induce a neutral gas drift velocity by ion collisions. The Lorentzian volumetric momentum loss term for ions is given by,

$$\dot{M}_i = M_i n_i v_{di} \nu_{in} = M_i v_{di} R_{ni} \qquad (22)$$

The neutral momentum acquired from the Lorentzian collisions with the ions is given by,

$$\dot{M}_o = M_o v_{oi} M \nu_{ni} = M_o v_{oi} R_{ni} . \qquad (23)$$

The ion mobility drift velocity is given by,

$$v_{oi} = \frac{eE}{M_i v_{in}} \qquad \text{meter/sec} \qquad (24)$$

Substituting equation (22) and (23) in equation (24), one obtains the neutral gas velocity induced by ion-neutral momentum transfer.

$$v_{oi} = \frac{M_i v_{di}}{M_o} = \frac{eE}{M_o v_{in}} \qquad \text{meters/sec} \qquad (25)$$

where v_{in} is the ion-neutral collision frequency. For the ions, the drift velocity induced in the neutral gas is equal to the ion mobility drift velocity.

2.2.4 Peristaltic Flow Acceleration

So far, two fundamental EHD flow mechanisms have been studied. The third mechanism is peristaltic flow acceleration, which is actively under study at the University of Tennessee's Plasma Sciences Laboratory. This peristaltic gas flow accelerator is described in US Patent No. 5,669,583 [13]. In the peristaltic flow accelerator, successive electrodes are energized at increasing phase angles so that a traveling electrostatic wave moves along the surface normal to the electrodes. For one periodic cycle, eight electrodes are attached on the dielectric panel, each with a 45^o phase angle with respect to its previous neighbor. The distance between electrodes is 10mm in this experiment. However, one can vary the gap in the range of 0.5mm to 10mm depending on the plasma operating conditions and tracking (surface electrical breakdown) limitations. Figure 2.3 illustrates the concept of traveling wave (peristaltic) flow propagation.

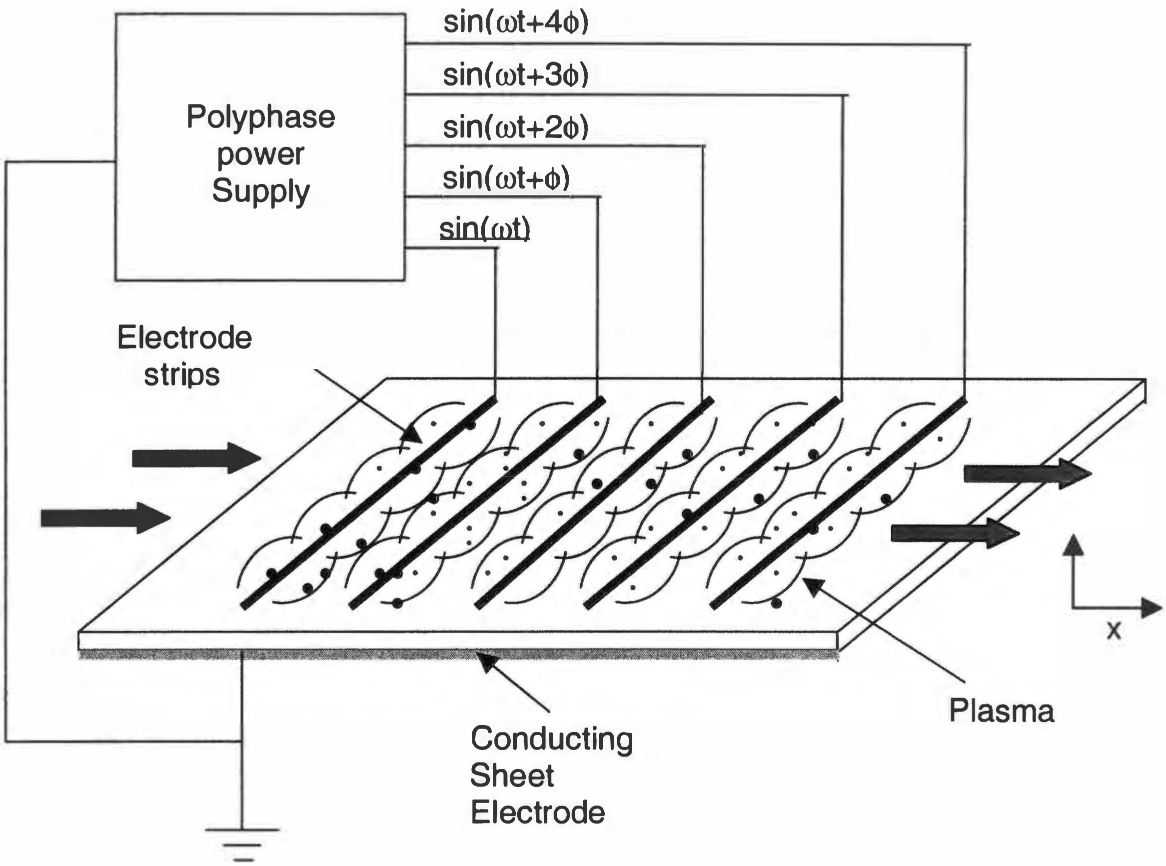

Figure 2.3 A peristaltic plasma accelerator with polyphase power supply. In our application, $\phi = 45^{o}$.

The potential of the traveling wave is given by,

$$V = V_o \sin(\omega t - kx) \qquad \text{volts} \qquad (26)$$

where the wave number is, $k = \frac{2\pi}{\lambda}$, the wavelength is $\lambda = NL$, N is the number of electrodes per cycle, and L is the distance between individual electrode centers.

The phase velocity acts on the net charge density, and is given by

$$v_p = \frac{\omega}{k} = \nu_o NL \qquad \text{meters/sec} \qquad (27)$$

where ν_o is the driving frequency in Hertz with typical operating parameters, ν_o = 3kHz, N = 8, L = 10mm, one can have a few hundred meters per second for the phase velocity. In order to match the phase velocity for best coupling of the ions to the traveling electrostatic wave, the ion mobility drift velocity should be of the same magnitude. The peristaltic electric field associated with the sinusoidal traveling wave is given as,

$$E = -\nabla V = V_o k \cos(\omega t - kx) \qquad \text{volts/m} \qquad (28)$$

The maximum electric field from equation (28) is $\frac{2\pi V_o}{NL}$, and the ion drift velocity is the same as the ion-induced neutral convection velocity from equation (25). This relation is,

$$v_{oi} = v_{di} = \mu_i E_{max} = \frac{eV_o}{M_i \nu_{in}} \frac{2\pi}{NL} \qquad \text{meters/sec} \qquad (29)$$

With typical operating parameters [18], one can calculate that the induced neutral gas drift velocity in atmospheric air is over 100 m/sec [17].

3. EXPERIMENTAL SETUP AND METHODS

The polyphase power supply system consists of a signal generator, phasing amplifier, power amplifier, and high voltage transformer, as shown on Figure 3.1. One may design the signal generator using analog or digital circuits depending on the operating requirements. When analog circuitry is utilized, an analog feedback circuit can be used to generate a phase difference. A digital signal generator can be constructed using an operational amplifier or computer-based software programming. The low frequency RF signal is amplified by a power amplifier. The amplification factor is adjusted to generate the desired voltage output at the transformer secondary with eight phases per cycle equally spaced at 45°. The frequency range is between 1 and 10kHz, and the voltage output should not be distorted when the output voltage at the final stage is maximum.

3. 1 The Multi-Channel Signal Generator

The required eight polyphase channels are provided by four separate sinusoidal signals spaced equally and successively by 45°, so that the leading output phases are 0°, 45°, 90° and 135°, or the reversed lagging series as shown in Figure 3.2. The voltage outputs must be set simultaneously by a single controller, and filtered so that voltage transients cannot propagate through the whole system. Suitable single signal generators with a single output are commercially available as research instruments. However, a multi-channel or polyphase signal generator is not available, and it must be designed using digital or analog circuits.

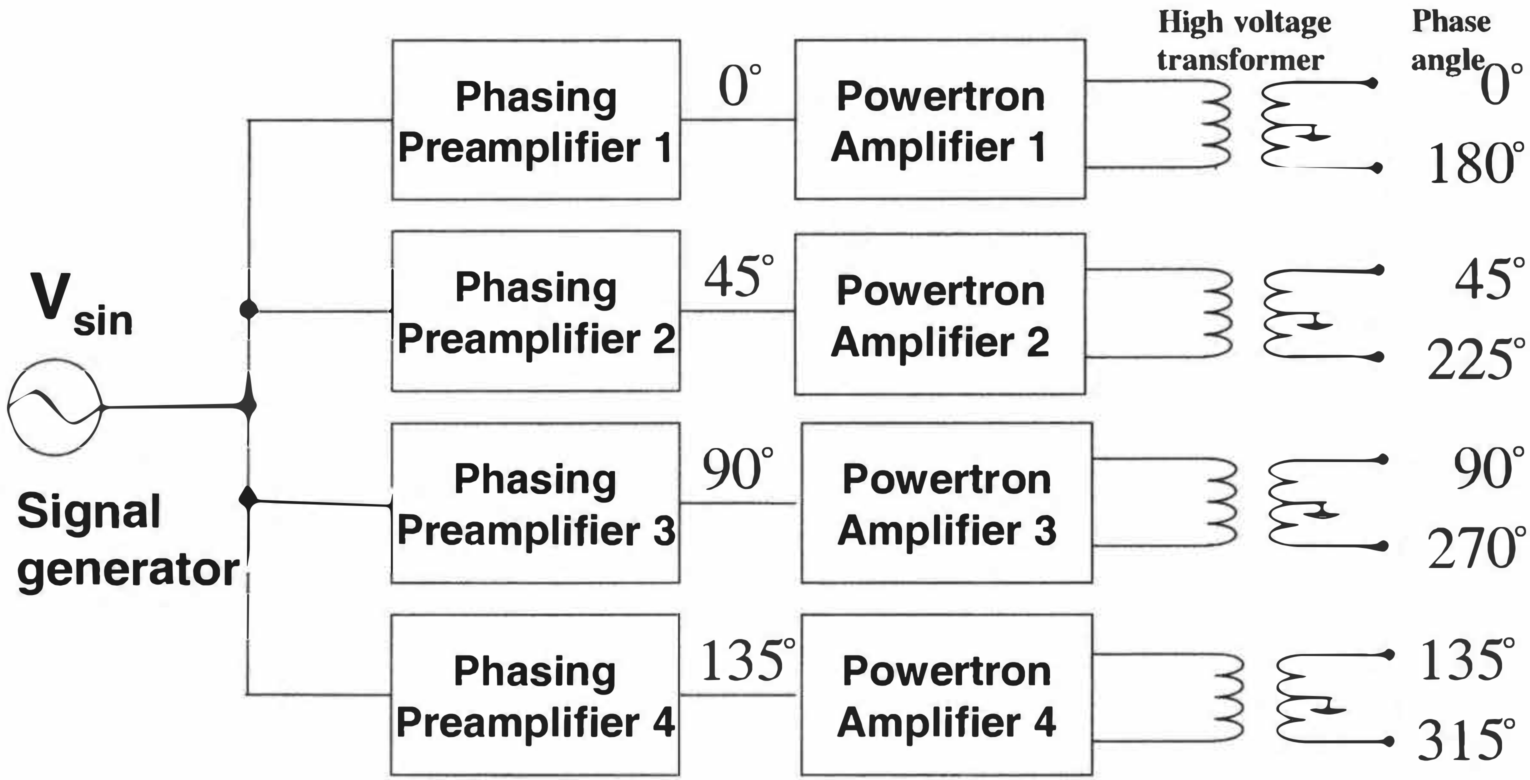

Figure 3.1. Schematic diagram of the power supply system for the peristaltic experiment.

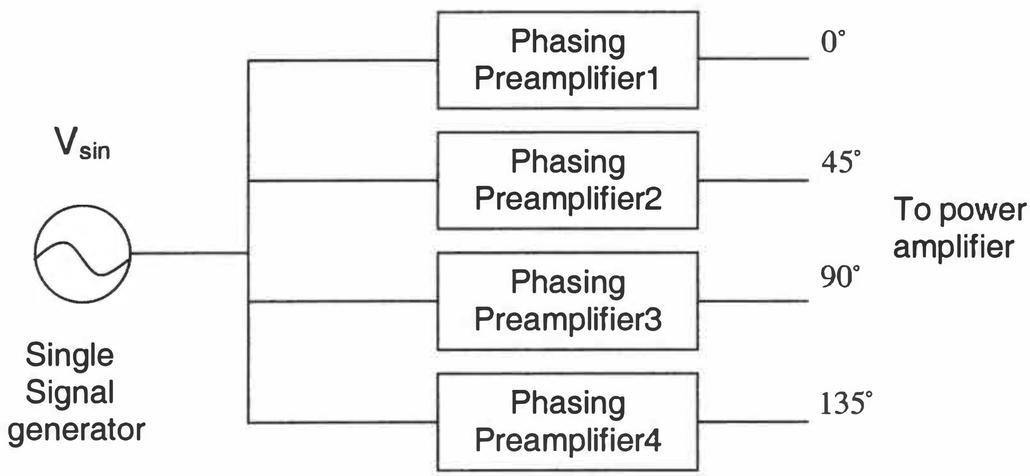

Figure 3.2 Signal feed system for the power amplifiers

An analog polyphase signal generator can be designed using feedback amplifiers that provide stable and strong output signals. The stability of the output signal is critical, because the polyphase signals can be affected by such sources of RFI as the feedback harmonics from the RF plasma driving frequency. A characteristic analog pre-feedback amplifier for a stable polyphase signal generator is shown on Figure 3.3.

The output from a commercial sinusoidal signal generator (Hewlett Packard, Model 3310A) is adjusted to provide an rms output voltage that ranges from zero to 2V peak-to-peak. The amplification factor

$$\text{Gain} = \frac{V_{out}}{V_{in}} \approx 1\,, \tag{1}$$

can be adjusted by using variable resistors, R_{21} in the circuit. The frequency response was determined to be near 1 MHz.

The design of the analog signal generator was such that it generated three polyphase channels with 45^{o} spacing in addition to the input (zero phase) channel. However, it was not easy to find values of circuit parameters to produce a 45^{o} phase shift for a four multi-channel device, since the proper values of capacitance and resistance were hard to obtain. By increasing frequency, the effect of the output voltage amplitude could be neglected according to Equation (1) since the frequency response is much higher than the operating frequency. The analog approach to the polyphase signal generator was therefore abandoned since it was not easy to find the correct values of resistance and capacitance for the construction of four parallel polyphase circuits.

A digital signal generator was designed and constructed based on the LabView software program. To use the LabView program, a AT-AO-6 CAD (1994, Part Number

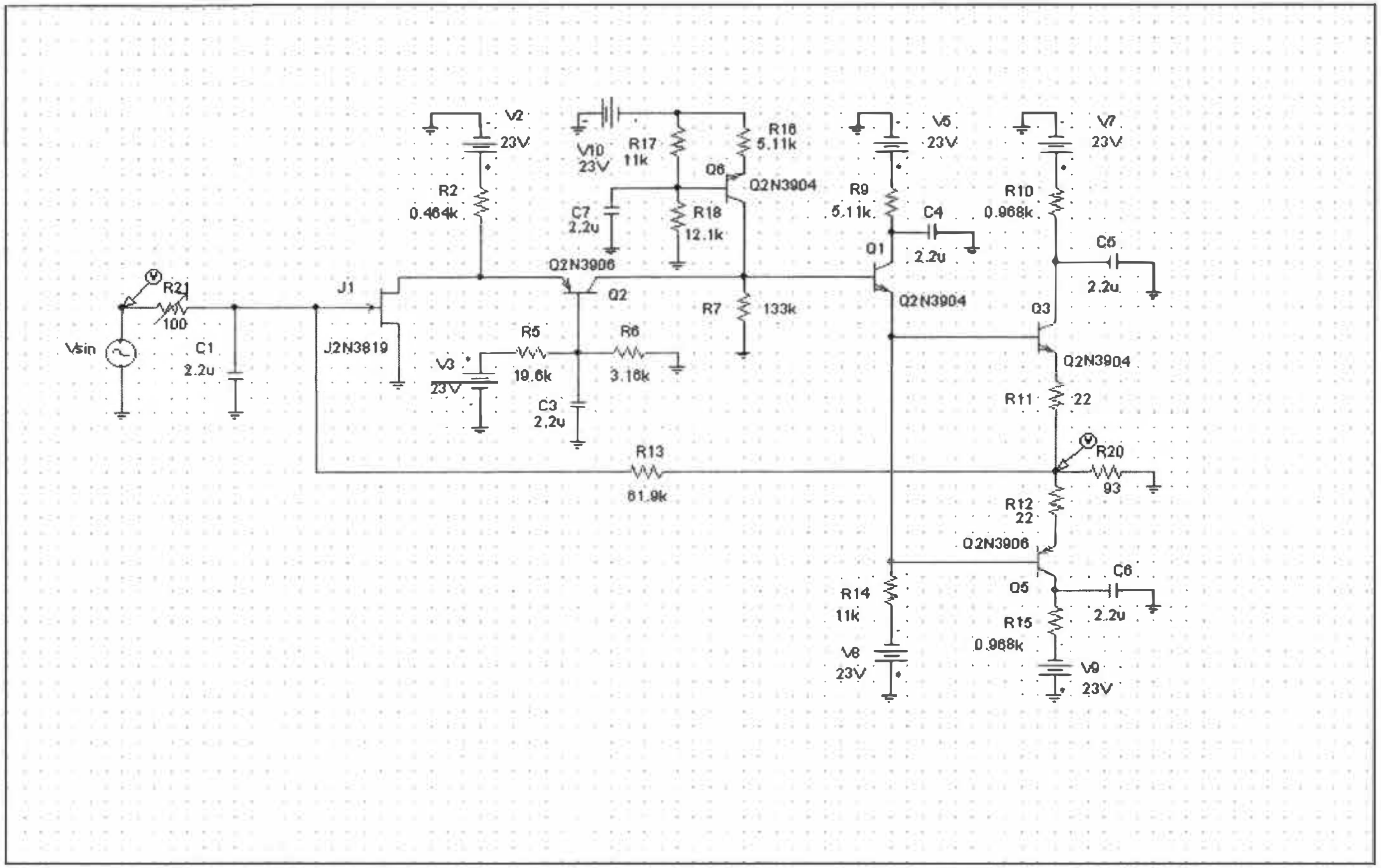

Figure 3.3 A feedback amplifier circuit for a multi-channel analog signal generator. This approach was abandoned in favor of digital signal processing.

320379-01 National Instrument, Inc) was installed to generate an analog output voltage. The CAD generates eight channels with a sampling rate of 330 kHz. The output is approximately sinusoidal for a single channel at 10 kHz output, but for four simultaneous channels at 10kHz, it produced a stair-case wave as shown in Figure 3.4. This stair-casing causes stress the power supply system, such as overheating of the solid state circuit components and the high voltage output transformer core. Although it had this limitation, the digital signal generator was used in this experiment because of its convenient operation illustrated on Figure 3.5 and Figure 3.6. The LabView microprocessor was programmed to generate four simultaneous sinusoidal channels with 45^{o} phasing. The amplitude of each phase, the DC offset, and the phase angle can be adjusted independently as shown on Figure 3.5.

3.2 Power Amplifier System

Following the polyphase signal generator is the RF power amplifier (Industrial Test Equipment Co., Inc, Model 1599CN). The radio frequency amplifier has an input range of 0 to 2.5V peak-to-peak, and a gain of 110 to 130 depending on the desired level of amplification. The upper limit of RF frequency is 20 kHz for the amplifier, and its maximum output voltage is 300V peak to peak. The amplifier consists of 24 pairs of p-type and n-type MOSFET transistors. A MOSFET transistor has a maximum power rating of 150W so that the RF amplifier can handle up to 1500W. Since the transistors are sensitive to heat and RFI, they were damaged during developmental testing at

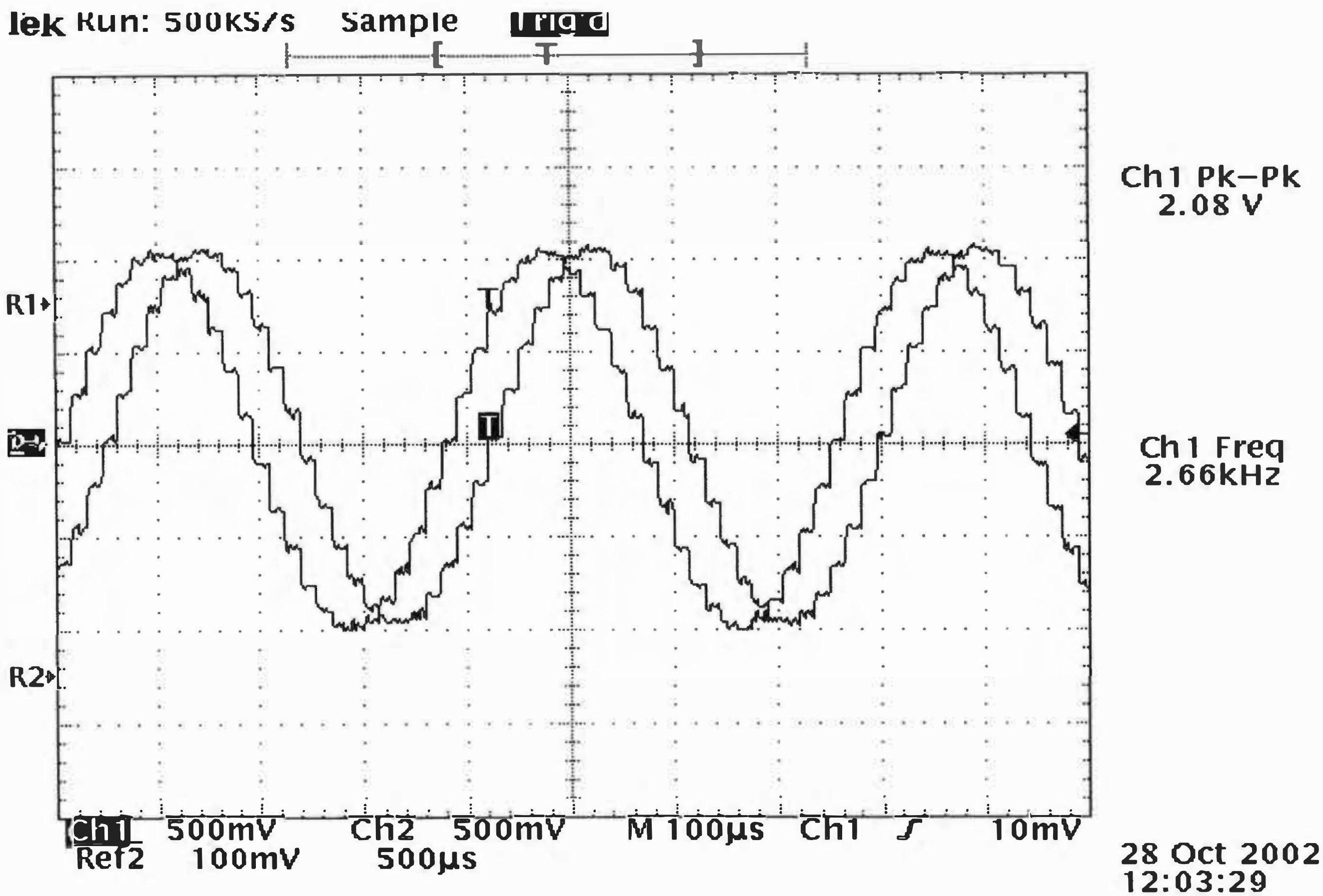

Figure 3.4 A stair-case example generated by AT-AO-6 CAD at 2.66 kHz and 2.08V peak-to-peak

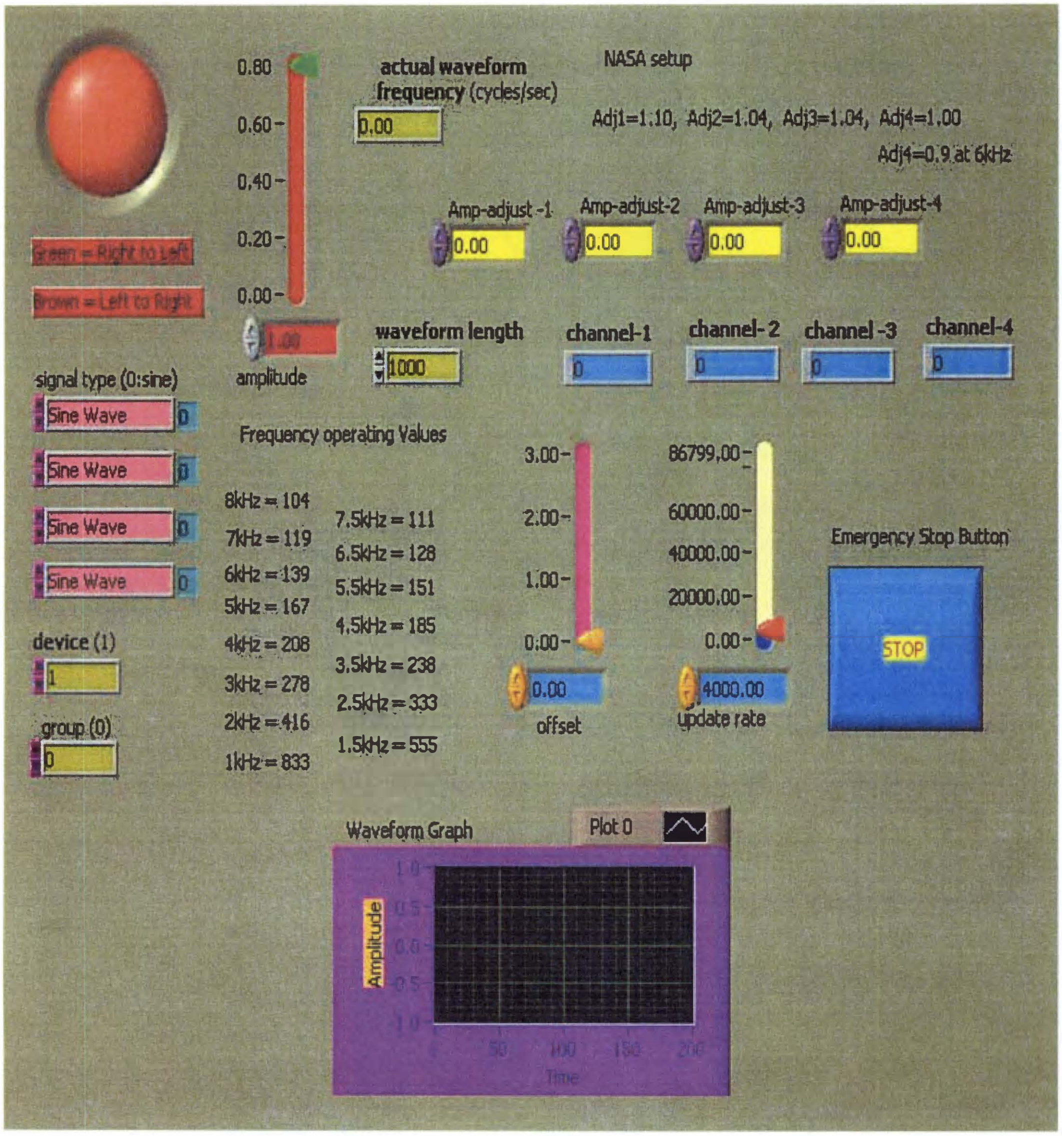

Figure 3.5 Polyphase signal generator control panel associated with the digital LabView software.

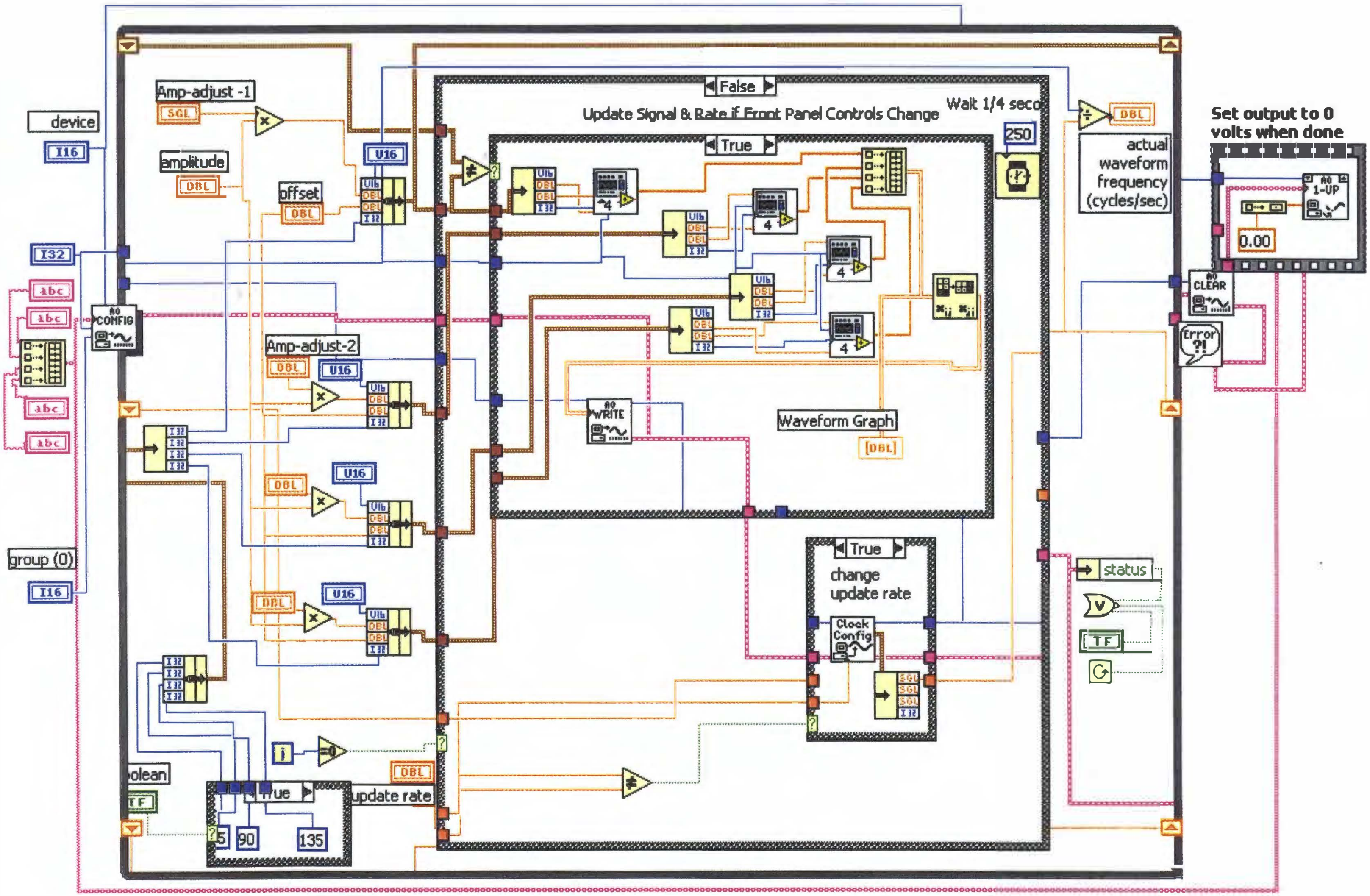

Figure 3.6 Flow chart of digital signal generator programming for the LabView

considerable expense and time. It was necessary therefore to be able to find the bad transistors by checking transistor characteristics.

Figure 3.7 is the schematic of a typical MOSFET, an aid in determining whether a particular unit is good or faulty. It is a simple matter to determine the resistance values external to the transistor, but not the internal resistance values. It was observed that determination of the resistance values in Figure 3.7 is not essential since other characteristics, such as capacitance and voltage (C-V) curves, and current and voltage (I-V) curves can reveal a faulty MOSFET unit. To determine the gate capacitance (C_{gs}), one should first connect the negative side to the source, and about 3-4 DC volts is applied to the positive side gate pin. Secondly, a positive potential should be connected to the drain, so that the transistor is turned on, and C_g is charged up to yield a low reading. The range of a low reading is between 0.35 and 0.37nF for the ECF10N20 type MOSFET used in the power amplifier. With the positive DC voltage still connected to the drain, the source and gate should next be grounded. The drain will be discharged and the reading will be higher than C_{gs}, indicating the device is functioning normally. The nominal range of C_{ds} is between 0.9 and 1.0nF for normal MOSFETs used in the power amplifier.

3.3 The High Voltage Transformer

Low frequency RF high voltage transformers are available on the market by special order. We used a model VT-35/RM-109 from the Industrial Test Equipment Co., with a turns ratio of 1:40. Since we want the output voltage to be over 5 kV_{rms} with frequency response up 10 kHz, serial connection of the transformers can be used to generate 5 kV_{rms}

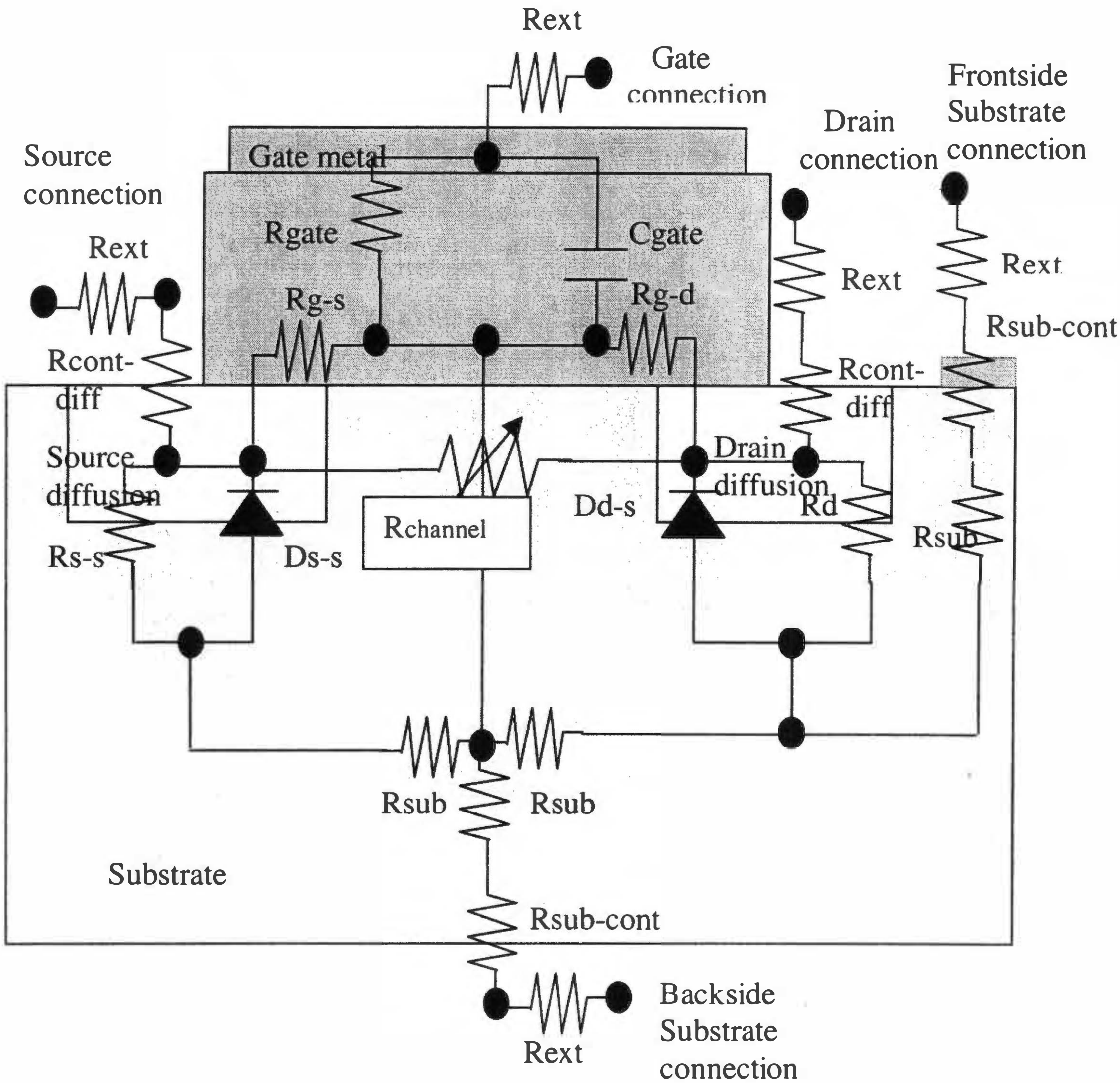

Figure 3.7 MOSFET schematic, where

Rext = external parasitic resistances.
Rsub-cont = contact resistance between metalization and the substrate areas.
Rgate = resistance of gate oxide insulator to substrate.
Cgate = capacitance of gate oxide.
Rg-s = resistance of gate oxide insulator to source.
Rchannel = gate voltage controlled effective resistance.
Ds-s and Dd-s = diodes formed by source-substrate and drain-substrate p-n junctions.
Rs-s and Rd-s = reverse-bias leakage resistance of source-substrate and drain substrate p-n junctions.
Rsub = substrate resistance.

with the center tap grounded, so it can give two voltage outputs with a 180^{o} difference in phase angles as illustrated in Figure 3.8.

The transformers were immersed in mineral oil to improve their resistance to high voltage breakdown during voltage spikes from RFI. The rms output voltage could be increased by 10 to 20%. Another approach to increasing the output voltage is to connect two transformers in series, so that the total output is 10kVrms for a single phase. This method decreases the frequency response of the series configuration due to capacitive effects.

The voltage output of the transformers was measured, and found to be linear with input. However, the output voltages of different transformers were not identical due to slightly different turns ratios in the transformers. Since the same rms voltages, only with different phases, are required for the experiment, the input signal was adjusted to produce the same output voltages. These results are shown in Figure 3.9 and 3.10.

3.4 The Peristaltic Accelerator Panel

We used two panel configurations to accelerate EHD flows. One is the symmetric peristaltic panel illustrated in Figure 3.11, and the asymmetric paraelectric panel illustrated in Figure 3.12. The symmetric peristaltic panel is used by applying polyphase voltages to the electrodes with a 45^{o} phase difference between them. The dimensions and spacing of electrodes on a symmetric panel can be varied to find the optimum operating condition without damaging the electrodes by sparking or tracking. In the experiment discussed in this thesis, the spacing between the electrodes is 10.0 mm, the width of each electrode is 1.0 mm, and the thickness of the dielectric panel is 1.0 mm. The thickness of

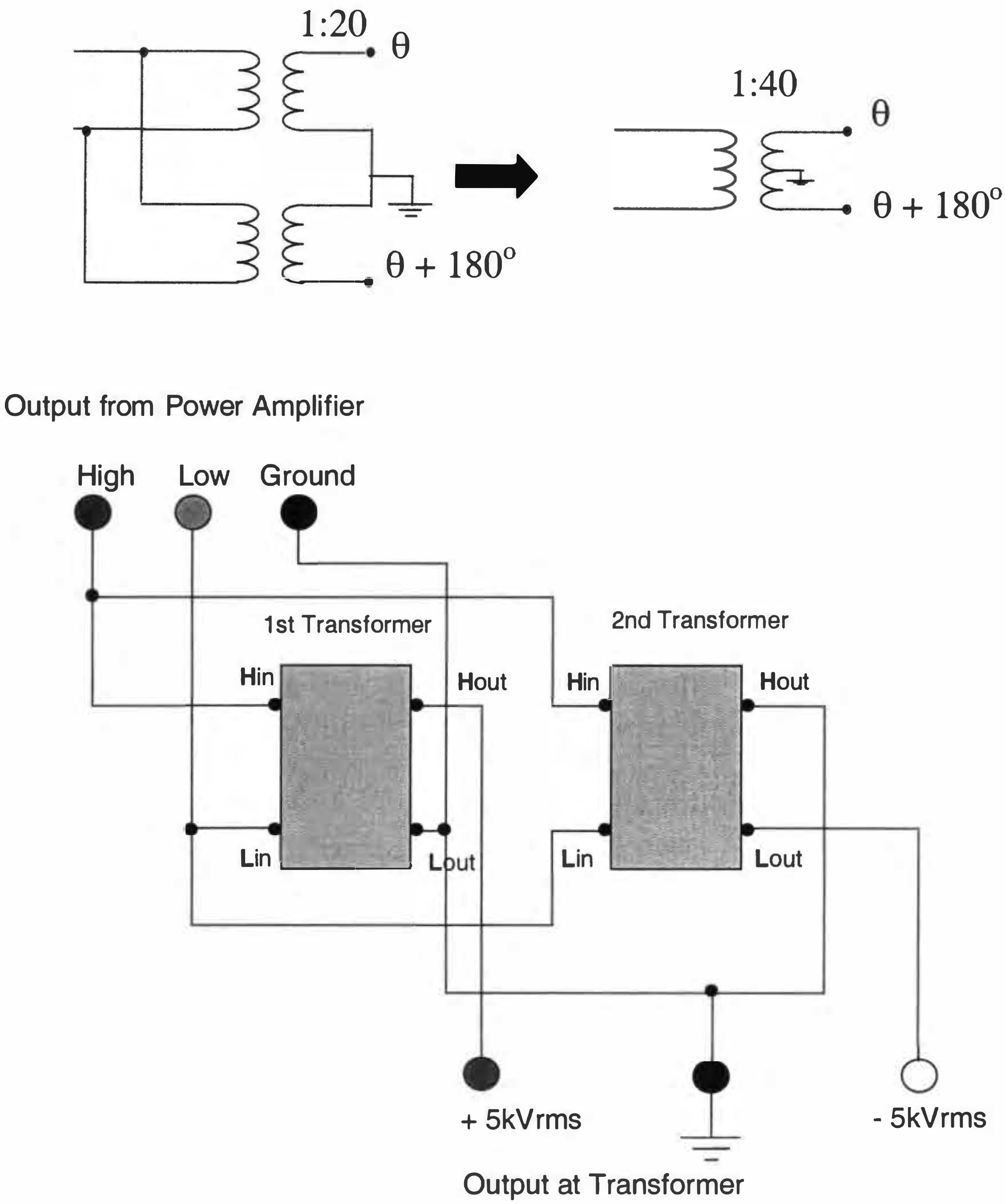

Figure 3.8 Two-transformer serial connection to give 10 kVrms with opposite phase angles.

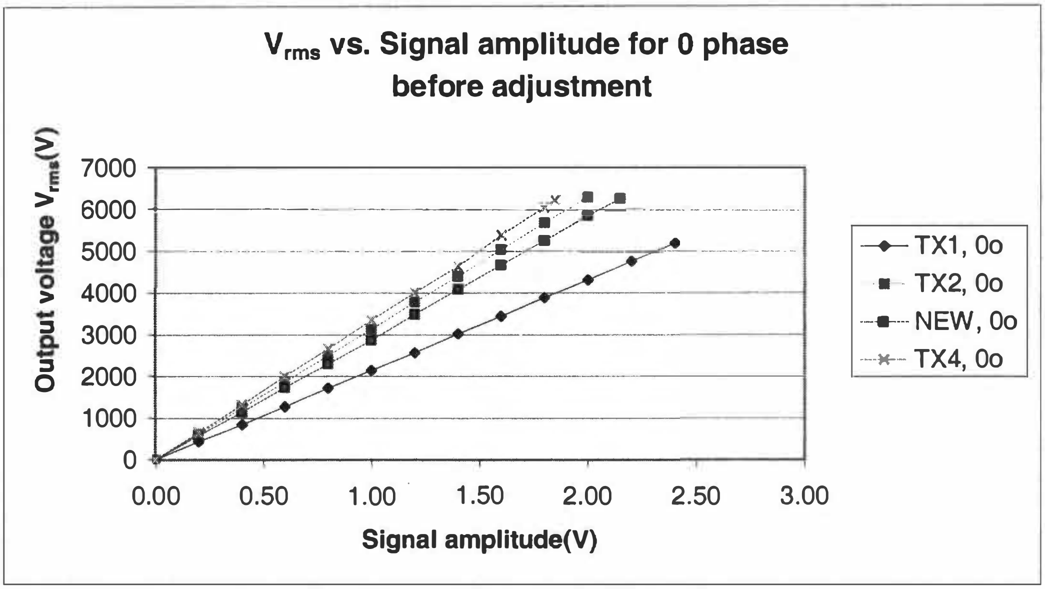

Figure 3.9 Voltage output of high voltage transformers before input signal adjustment. It shows a linear increase of the output for each transformer at 3 kHz

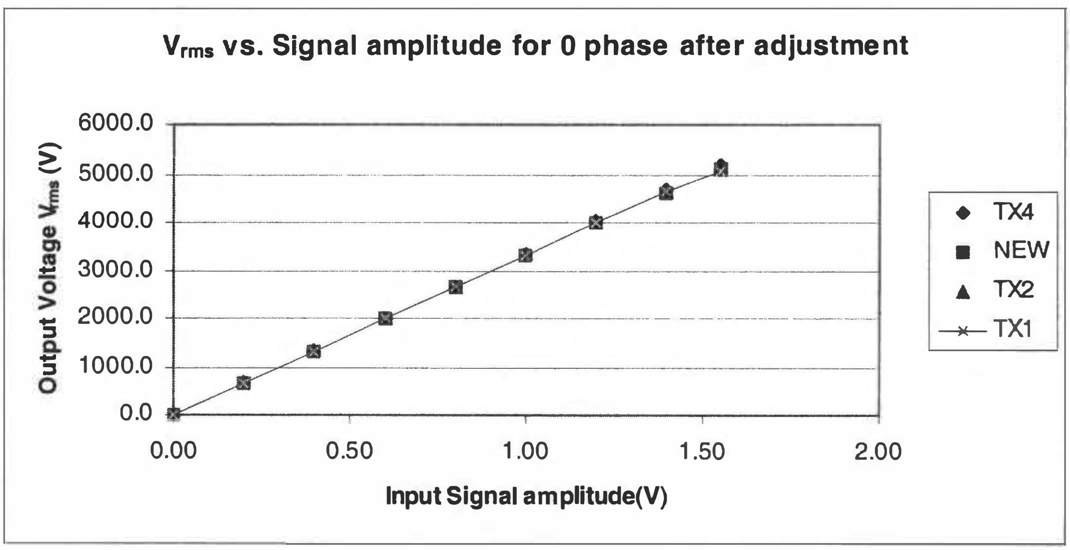

Figure 3.10 Voltage output of high voltage transformers after input signal adjustment. It shows an identical linear increase of the output for each transformer at 3kHz.

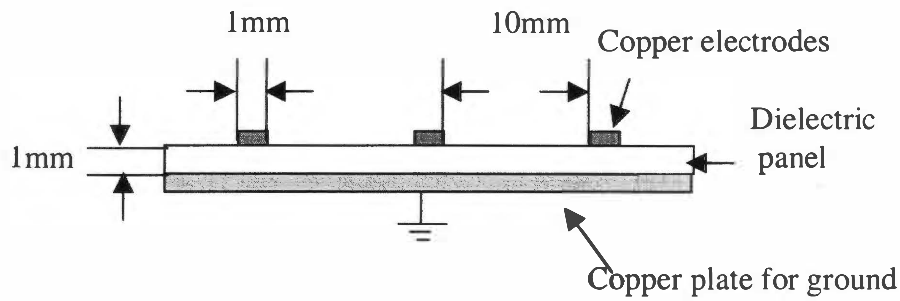

Figure 3.11 Symmetric panel configuration used for peristaltic flow acceleration.

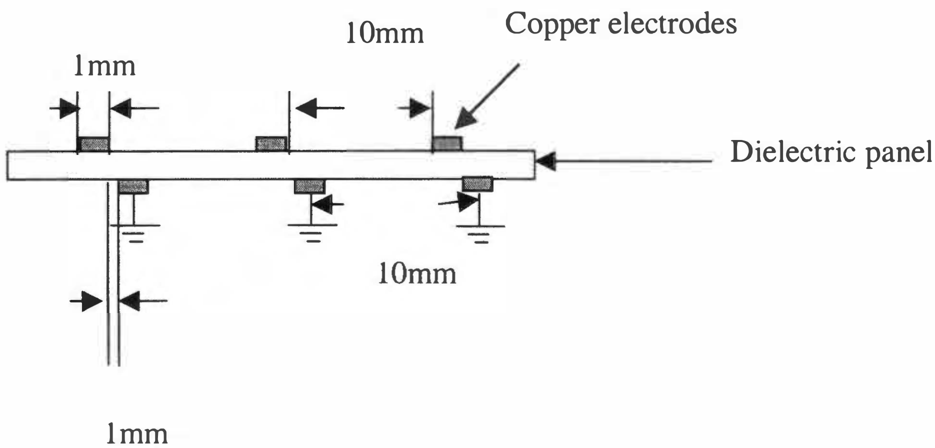

Figure 3.12 Asymmetric panel configuration used for paraelectric/peristaltic flow studies.

the copper electrodes (and their height above the panel surface) was 0.040 mm. The dielectric panel was made with a polyimide circuit board that has a relatively high dielectric constant.

The asymmetric panel shown in Figure 3.12 can be used for paraelectric flow acceleration experiments that demonstrate flow attachment to airfoils. An asymmetric panel may also be used to study the combined effect of paraelectric and peristaltic flow acceleration on the electrodes. The asymmetric panel was used only for paraelectric flow acceleration measurements not reported in this thesis.

A schematic of the polyphase connections to the symmetric peristaltic panel is shown in Figure 3.13. The phase angle of the driving voltage on successive electrodes is increased by 45^{o}. It consists of three complete cycles so that the peristaltic flow can been seen after damping of starting transients. This panel was used to obtain the peristaltic flow data discussed below.

A great deal of development work was required to overcome tracking and sparking problems, causing delay of the experiment. The main reason for these problems is the undesired current from voltage transients that reach the electrode before initiation of the plasma. The value of the current was measured in the range of 600 – 700mA. The current can be reduced by applying a shunt resistor to the electrode, as shown in Figure 3.14. After adjusting all the elements of the peristaltic flow acceleration system, experiments can be performed. In order to conduct such experiments safely, one must avoid danger associated with high voltage. A schematic of the over-all system is presented on Figure 3.1.

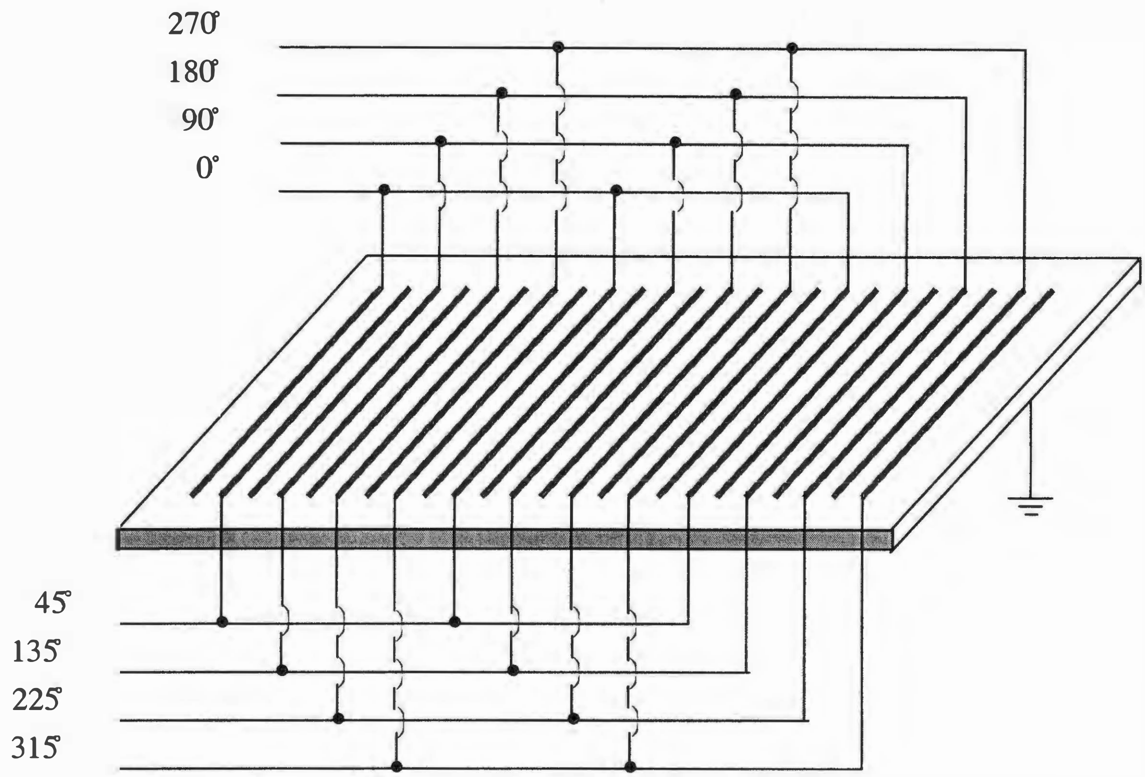

Figure 3.13 Electrode phase connections for the peristaltic accelerator panel of Figure 3.11. A copper sheet electrode covers the bottom surface of the panel.

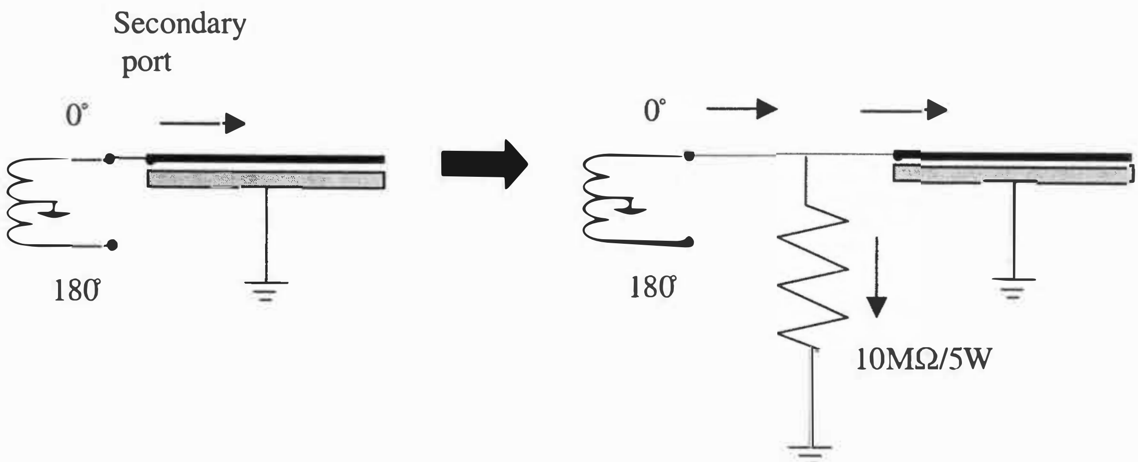

Figure 3.14 A method to reduce transient current flow to the electrode.

3.5 The Smoke Generation System

One needs a smoke generation system to visualize the peristaltic flow on the panel. The smoke chemistry should not damage the panel and it should not disturb the flow, while revealing the aerodynamic flow lines above the panel. The use of titanium tetrachloride ($TiCl_4$) for this purpose is standard in aeronautical research, since titanium dioxide smoke is not toxic to humans. The chemical reaction is as follows, where the water is provided by the humidity in normal atmospheric air.

$$TiCl_4 + 2H_2O \rightarrow TiO_2 + 4HCl \quad (2)$$

The production of smoke is accomplished with the arrangement shown schematically in Figure 3.15. The byproduct, hydrochloric acid vapor, corrodes many materials. The end of the nozzle and the electrodes on the panel can be damaged by this byproduct, and it can affect the flow by its formation as a liquid on the panel. This problem can be avoided by bubbling the smoke through a water bath prior to injecting the smoke into the flow. This is done by attaching an additional flask containing water, as illustrated in Figure 3.16. Since hydrochloric acid is very soluble in water, but the titanium dioxide smoke is not, the output is relatively pure titanium dioxide smoke. One may use pressurized air to make the gas denser. The pressure is adjusted so the smoke is a gentle stream at the output nozzle.

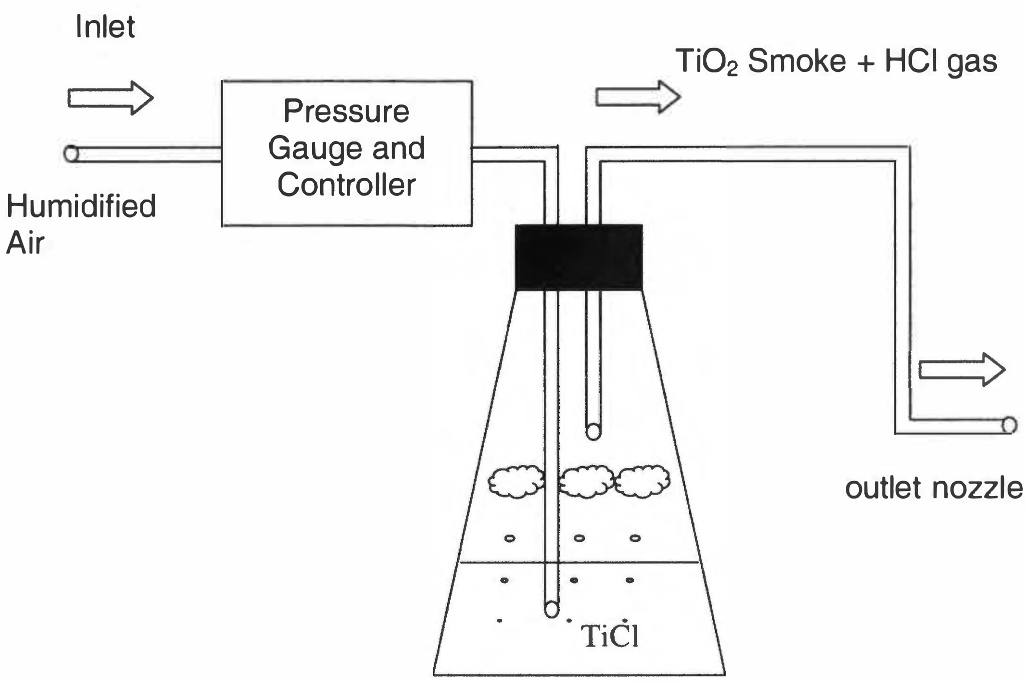

Figure 3.15 Smoke generating system using titanium tetrachloride ($TiCl_4$).

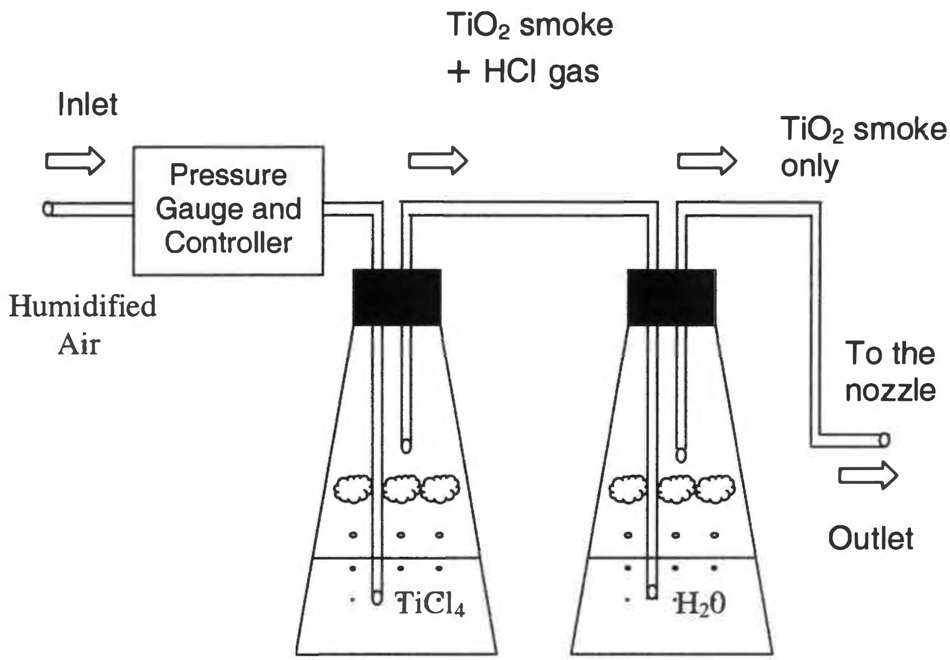

Figure 3.16 Enhanced smoke generation system for removal of hydrochloric acid.

3.6 Velocity Measurement System

For simple gas flow measurements, a Pitot tube can be used as shown on Figure 3.17. The relationship between the measured pressure and velocity is described by Bernoulli's equation, where the static pressure plus dynamic pressure is the total pressure, a constant.

$$p_s + \rho\frac{v^2}{2} = p_t \qquad (3)$$

In this expression, p_s is the static pressure, ρ is the air density, v is the measured speed, and p_t is the total pressure.

Solving this equation for velocity, one obtains

$$v = \alpha\sqrt{p_t - p_s} \qquad \text{m/sec} \qquad (4)$$

where the unit of pressure is usually in Torr. Since the pressure generated by the peristaltic flow and measured by a Pitot tube is related to the speed of the flow by the square root of the pressure, one must calibrate the Pitot tube to find its instrumental constant. In our experiment, the instrumental constant for our Pitot tube system was found to be 14.48. Direct Pitot tube measurements can provide accurate velocity profiles of the boundary layer flow.

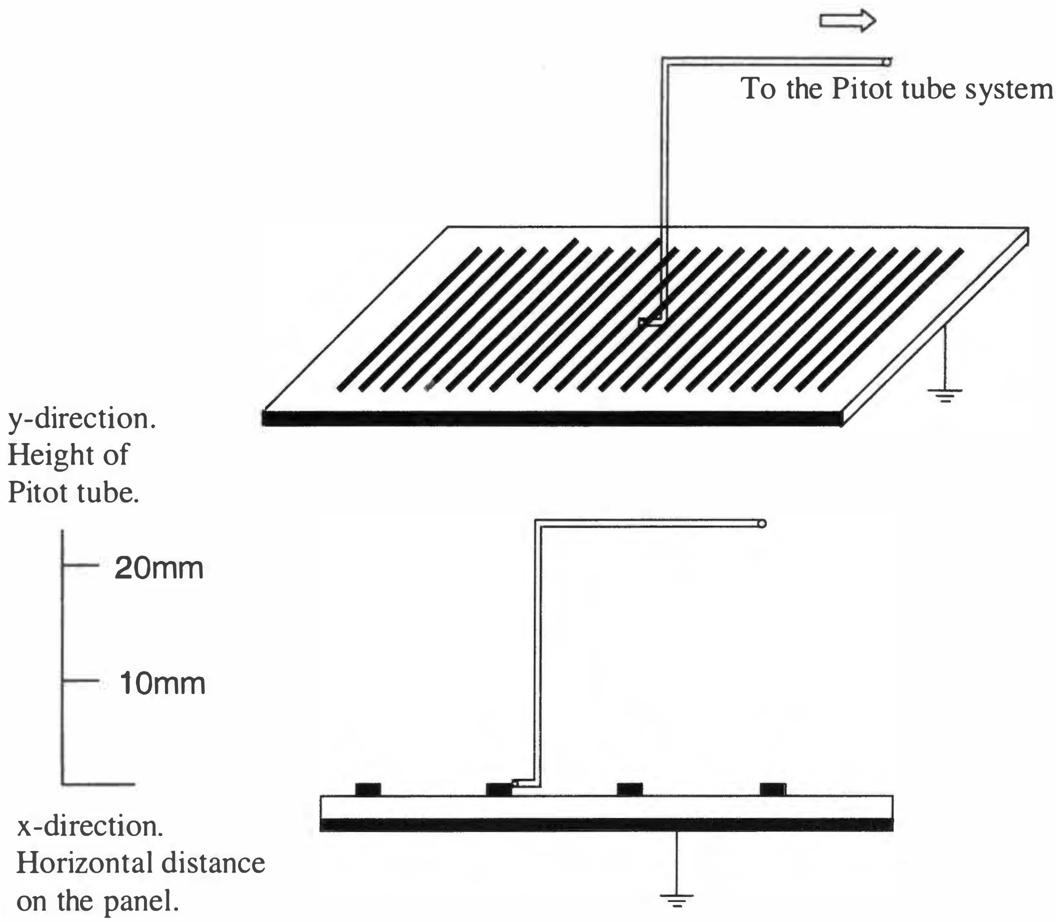

Figure 3.17 Pitot tube system. The distance between electrodes is 10 mm
The height of electrode is negligible.

4. OBSERVATIONS AND RESULTS

4.1 Observed Features of the EHD Flow

The One Atmosphere Uniform Glow Discharge Plasma (OUAGDP^{TM}) has been generated using a polyphase power supply system. The space between the centerlines of two adjacent electrodes was 10 mm in these experiments. The phase angles start out from zero degrees and go to 315^{o} in increments of 45^{o} in one complete cycle. The peristaltic panel used for the data presented in this chapter has three complete cycles with 24 electrodes. The direction of the induced gas flow can be adjusted from left to right and vice versa by operating with forward or reversed phasing. The back side of the panel is a grounded copper plate. The dielectric panel between the electrodes and the grounded plate is a polyimide-glass circuit board with a high dielectric constant of 4.0-4.6 relative to air. The thickness of the dielectric is 1.0mm.

Figure 4.1 shows the generation of a peristaltic plasma using the polyphase power supply system. Before titanium dioxide smoke was used to visualize the peristaltic flow, fine powders were used as a flow diagnostic. The fine powders were deposited between two adjacent electrodes in long linear lands, like snowdrifts. In Figure 4.2, the peristaltic flow is not shown, only the deposition of the powder. One cannot determine the processes responsible for the powder deposition conclusively. It could be the paraelectrically induced flow between electrodes, or undesired heat from the panel near the electrode. The plasma-generated heat was not removed by active cooling, and may have affected the flow near the panel.

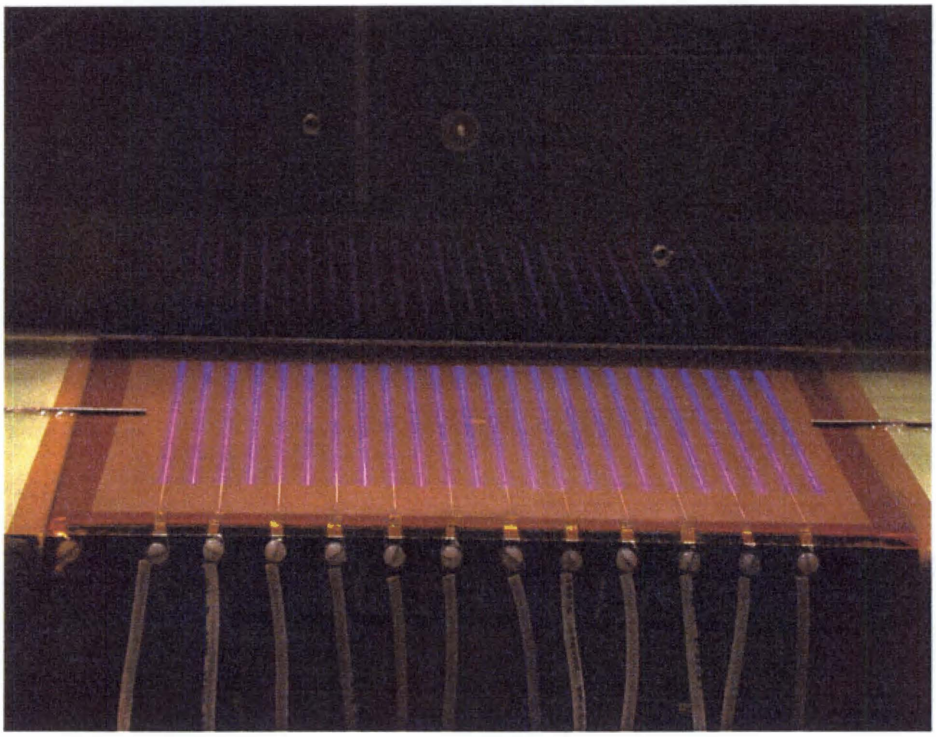

Figure 4.1 OAUGDP^{TM} generated on a peristaltic panel using an eight phase polyphase power supply with 3.5 kV_{rms} at 3kHz. Note the Pitot tubes to the right and left.

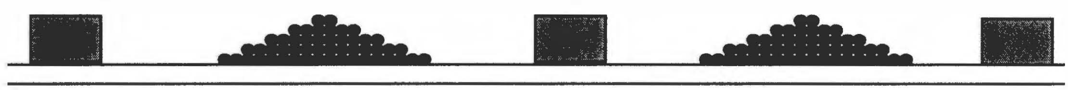

Figure 4.2 The scattered powder formed linear lands between the electrodes after plasma generation with polyphase RF power supply.

Titanium dioxide smoke was used to visualize the flow and was applied by a probe that terminated 2.5 cm above the panel as shown in Figure 4.3. These pictures differ only in the phasing of the electrostatic wave, being left-to right (positive) in Figure 4.3 (a), and right-to-left (negative) in Figure 4.3 (b). Clearly, one can see the reversed flow direction when the phasing is reversed.

Figure 4.3 (a) and (b) clearly confirm the peristaltic flow by demonstrating the effect of reversed phasing. One can retrieve the video files of this peristaltic smoke flow test by visiting the website http://plasma.ece.utk.edu/ and clicking on the video clips. From Figure 4.3, careful observation of the boundary flow shows that the smoke flow is quasi-sinusoidal, not one-dimensional straight flow lines. Figures 4.2 and 4.3 can be used to propose the flow model sketched in Figure 4.4. A better model could no doubt be obtained by PIV (Particle Imaging Velocimetry) measurements, but even this method is not definitive since particles on the panel cannot be detected.

The distance between the steady flow at the top of the diagram in Figure 4.4 and the top surface of the panel was about 10mm. The results of the flow model are somewhat crude. However, one can identify several points for future study. One knows that the highest electric field occurs near the electrodes, where paraelectric effects may be dominant, and that heat from the plasma near the electrodes may play a role. Since the Pitot tube velocity measurements were limited, the entire *vertical* velocity profiles are not available at this point. Approximately 100 data points are required to determine the velocity profiles using the Pitot tube measurements in the two-dimensional space between two adjacent electrodes for steady-state flows.

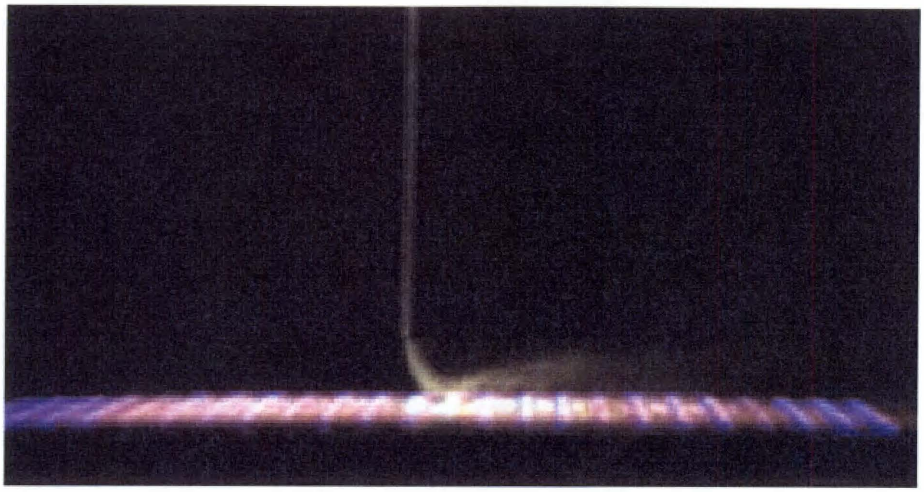

(a)

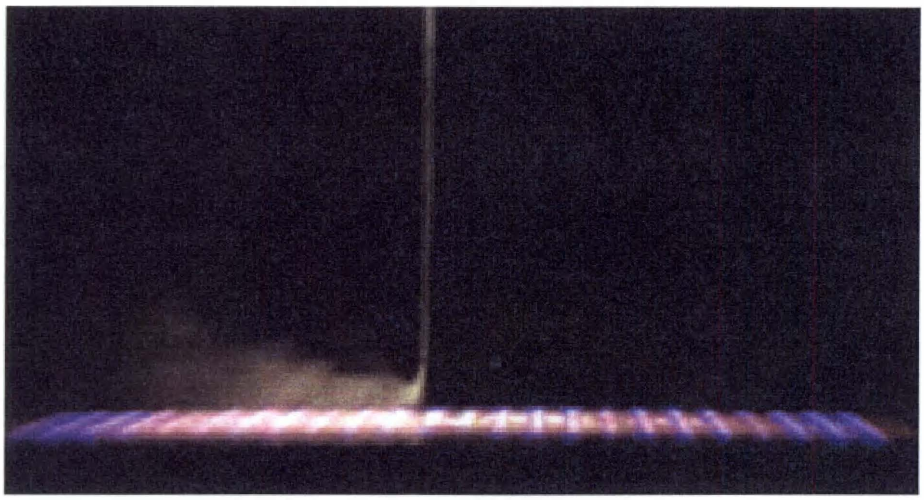

(b)

Figure 4.3 The visualization of peristaltic flow using titanium dioxide smoke. Voltage applied to the electrode is 3.5kVrms at 3kHz frequency with three complete phase cycles on the panel. (a) The phase angles were increased by 45° from left to right, (b) Exactly same condition as (a) except that phasing was reversed, with the phase angle increasing by 45° from right to left.

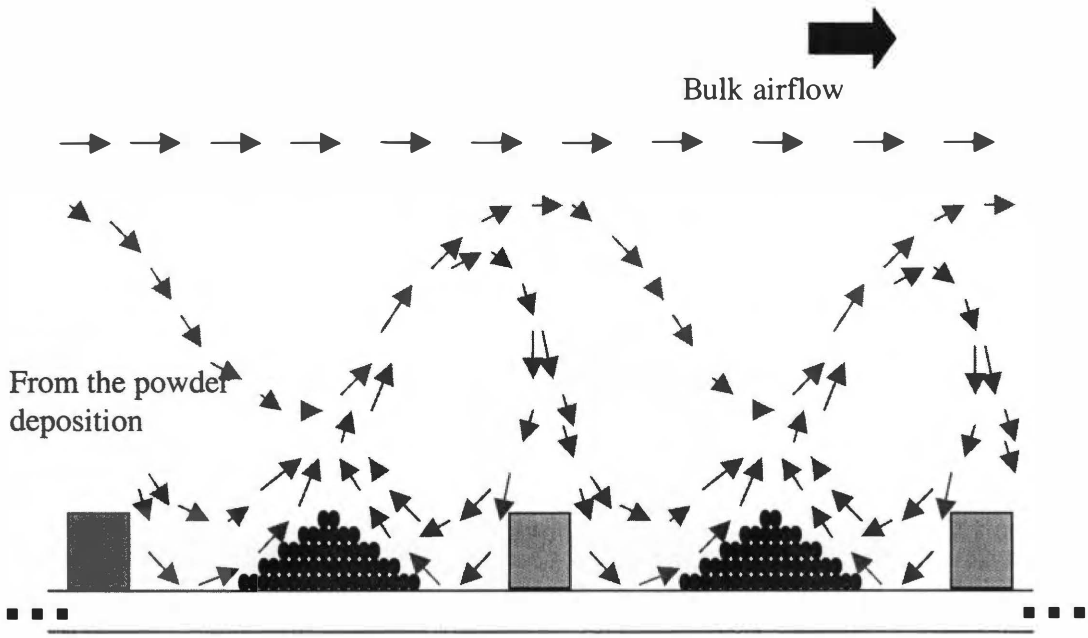

Figure 4.4. Proposed flow model near the panel using both powder deposition from Figure 4.2 and smoke flows from Figure 4.3. Not scaled.

4.2 Effects of Frequency and Electric Field on the Flow Velocity

The magnitude of the horizontal velocity as the applied voltage (and hence applied electric field) increases was measured at several frequencies. These data are plotted in Figure 4.5 above the panel. It was observed that the flow velocity increased at higher electric fields and frequencies, although the frequency dependence is non-monotone.

Boundary layer velocity profiles were taken by increasing the height of a Pitot tube above the panel surface. According to the flow model of Figure 4.4, the magnitude of the flow velocity cannot be same at the different heights above the panel. This effect is illustrated in Figure 4.6, where the non-monotone boundary layer velocity profile may be the result of vertical motions in the gas flow.

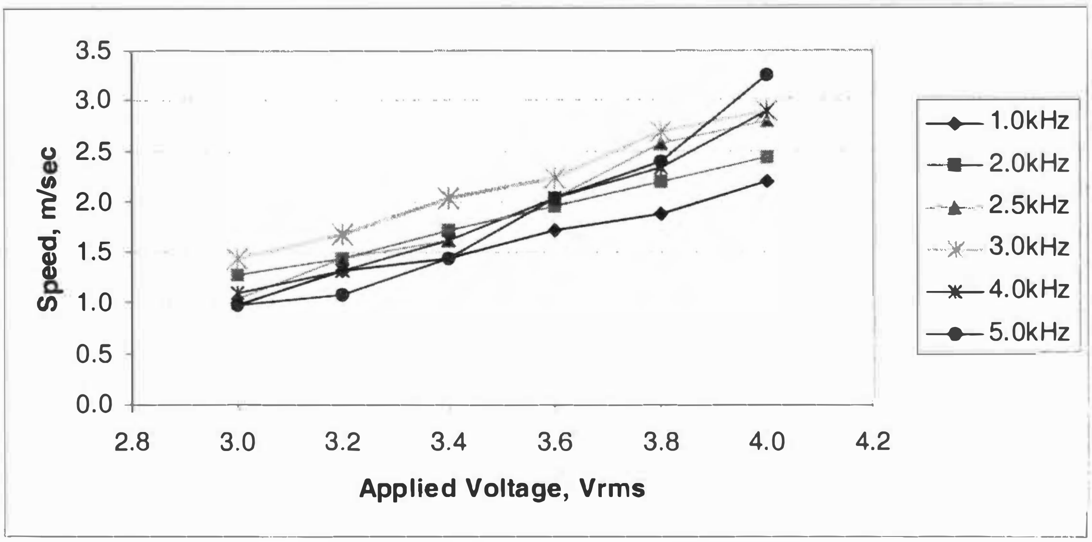

Figure 4.5 Flow speed as a function of applied voltage and RF driving frequency. The speed was measured with a Pitot tube. The location of the Pitot tube is shown on Figure.4.1.

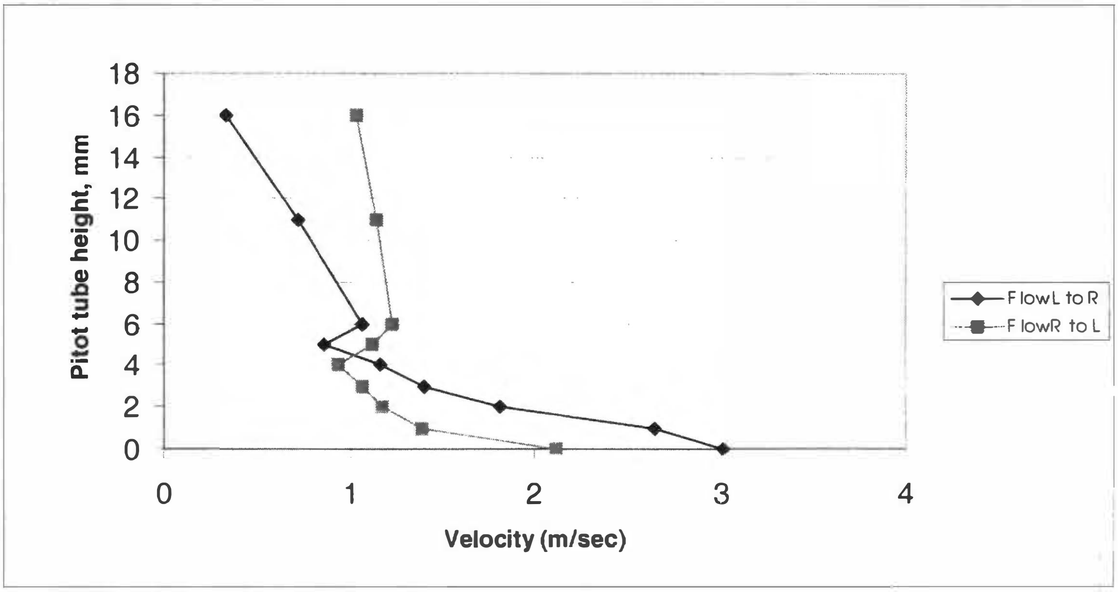

Figure 4.6 Magnitude of the EHD-induced boundary layer velocity profiles for forward and reversed peristaltic flow. The location of the Pitot tube was moved vertically above the peristaltic panel, as shown in the photograph of Figure 3.17 and 4.3.

5. DISSCUSION AND FUTURE WORK

Although the polyphase power supply can supply output voltages with eight phases up to 6 kVrms, the system is not stable at higher voltages because of tracking and sparking problems. These problems will be significant if a peristaltic panel is used for aerodynamic applications. There are several points to discuss regarding these problems.

First, the polyphase signal generator must provide a stable output signal. Although the Labview digital generator can provide almost perfect (i.e. nearly sinusoidal) signals by upgrading the computer CAD (at considerable expense), the output signal can be affected by RFI. The desired signal plus the RFI pass into the power amplifier and transformer, stressing both components and causing voltage spikes. These voltage spikes induce sparking and tracking on the panel. An analog signal generator would be ideal, but its construction is not easy. The feedback amplifier used in an analog signal generator can provide very strong desired signals, so that RFI cannot affect the signals input to the power amplifier and transformer.

The RFI comes from the surroundings, including the OAUGDP™ on the panel itself. A significant source of RFI that affected the input signals was RF harmonics generated by the plasma panel, which appeared on the signal generator. This problem was greatly reduced by shielding and related good practices, but additional filtering and shielding would be beneficial.

Second, the power transistors can be upgraded by purchasing a higher power rating (250W/220V). The power supply amplification factor is a primary characteristic of the power supply system, and higher values can provide a stable output voltage to the transformer to provide greater output.

Third, the heat generated on the panel by voltage transients will affect the flow and damage the panel, which is made with a high dielectric constant material. The undesired current flows during voltage spikes were reduced by ohmic heating in the 10 MΩ/5W shunt resistor shown in Figure 3.14. Optimization of the performance of the shunt resistors should be more thoroughly investigated.

Last, the most important part is to design a high voltage protection circuit using a diode, as shown in Figures 5.1 and 5.2. It was observed that when RFI was generated, it fed back through the power supply system, and was observed on the RF signal output. Obviously, such RFI may damage the whole power supply system. With this condition, it is not advisable to operate near the maximum voltage output, 7-8 kV_{rms}. One may construct an impedance matching circuit to avoid this problem, but the impedance matching systems require physically large and heavy coils and capacitors. Impedance matching, however, is the ideal case for delivering maximum power to the load [2]. Since the OAUGDP™ does not require maximum power from our power supply system, the impedance matching method was not adopted. Instead, one would like to construct the high voltage protection system with light electrical parts. A diode with a large breakdown voltage (A "lightning arrestor") could be good choice and may be available for purchase on the market.

It is a simple matter to construct a protection system if DC operation is used. However, AC operation is required in the peristaltic experiment, and it is not a simple matter to design and construct a protection system. Additional study and design should be devoted to installing a protection circuit on the on the secondary output terminals of the high voltage transformers. In Figure 5.3, the proposed circuit will allow two phase RF

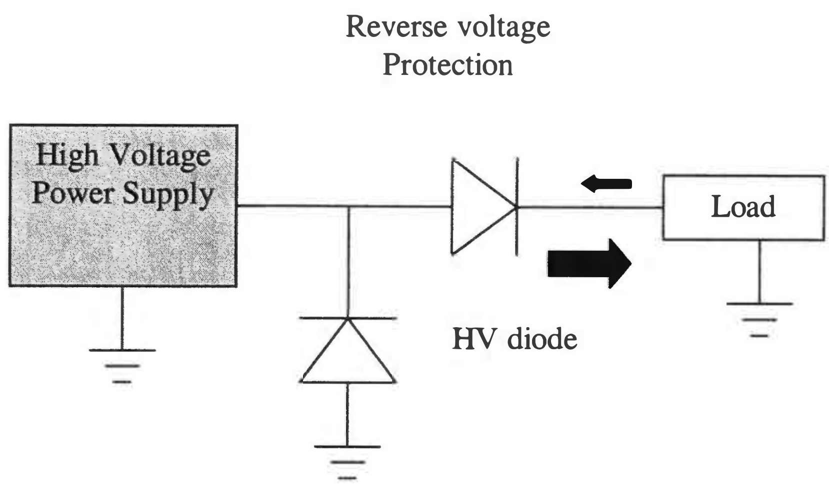

Figure 5.1 High voltage protection system using a diode for DC operation.

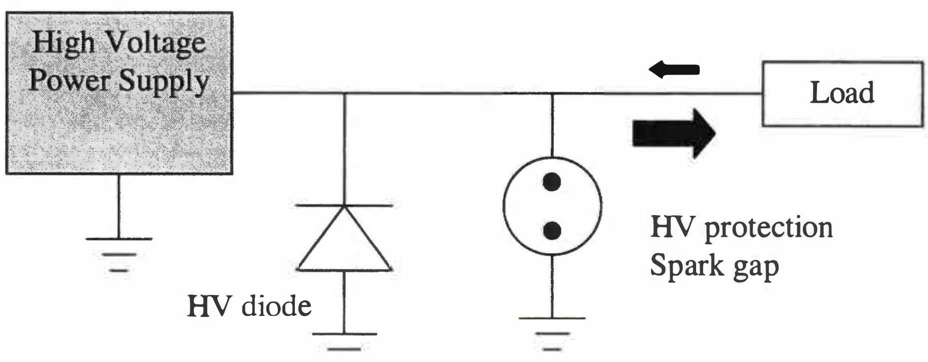

Figure 5.2 High voltage protection system using a spark gap for DC operation

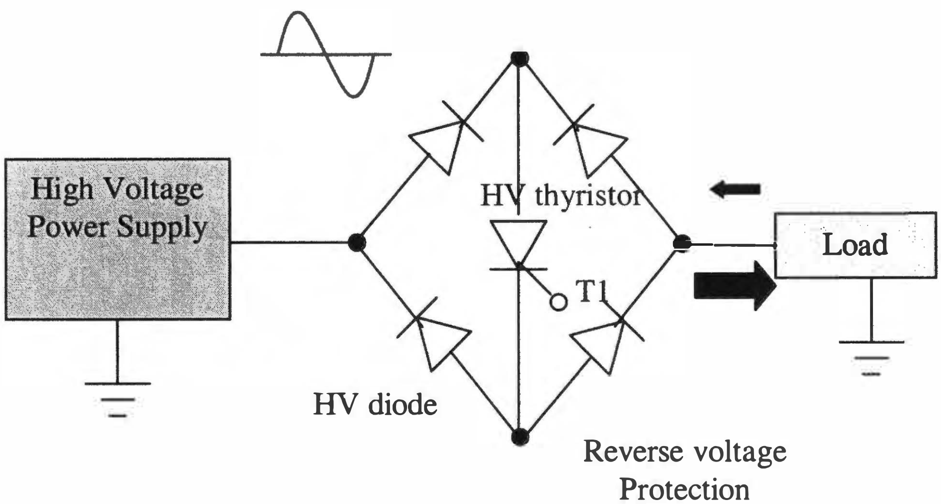

Figure 5.3 High voltage protection system using a bridge rectifier and thyristor for AC operation

transformer oil. This method cannot provide output up to 6kVrms because of the power amplifier limitation. Since an output voltage up to 7-8 kVrms is desirable for each electrode, one needs to add another transformer connected in series. As shown in Figure 3.8, if two or more transformers are added in series, the output voltage can be increased over 10kVrms; however this method will reduce the frequency response by half due to series connection of capacitance in the transformer.

The horizontal gap between the electrodes needs to be reduced to increase the RF electric field. One expects higher peristaltic flow velocity with higher electric fields. Since the plasma sheath is between 1.5 and 2mm, one can reduce the distance between electrodes about 5mm. Also, such electrode dimensions as width and thickness can be optimized to find the best operating conditions.

Flow velocity profiles using the Pitot tube are needed for further flow analysis. Crude flow velocity profiles are shown on Figure 4.6. If these velocity profiles are consistent with Pitot tube measurements taken at other locations between electrodes, one may see vortex formation at some locations.

6. CONCLUSION

A polyphase power supply system was constructed that is capable of generating eight phases of sinusoidal voltage output up to 6 kV_{rms}. The power supply system is composed of a signal generator system, power amplifiers, and high voltage transformers. Its frequency response was designed to be 10 kHz and the maximum voltage output can be up to 12 kV_{rms} without a grounded center tap. The polyphase power supply system successfully generated OAUGDP™ up to 5 kV_{rms}, the normal operating condition to generate the atmospheric glow discharge plasma in air. The polyphase signal generating system used to provide input to the amplifiers was designed using a LabView software program. The frequency response of the signal generating system is approximately 10 kHz, in the proper range for peristaltic flow testing. For further research, one should design and construct a RFI stabilizing system and a power supply protection system from RFI.

It is essential to visualize the peristaltic flow using smoke. The smoke generating system should not damage the peristaltic panel with its by-products, and a method has been developed using the solubility of HCl in water. The chemical reaction between the peristaltic panel and the by-product should be avoided to reduce arcing and tracking problems.

Demonstration of the peristaltic flow acceleration effect has been successful using forward and reversed RF phasing. The best method to diagnose the flow may be to use PIV (Particle Imaging Velocimetry). However, it is possible to suggest the peristaltic flow model of Figure 4.4 based on the current experiment. This flow model can provide a basis for further research. If generating peristaltic flow at higher subsonic velocities is successful, there may be innovative applications to aeronautical systems.

REFERENCES

1. Carr A., and Roth, J. R., *"Characteristics of a One Atmosphere Uniform Glow Discharge Plasma".* IEEE Paper 2HP-23, 23rd IEEE Conference on Plasma Science, June 3-5.

2. Chen Z, Morrison J, Ben Gadri R., and Roth, J. R., *"Low Frequency Impedance Matching Circuit for a One Atmosphere Uniform Glow Discharge Plasma Reactor",* Paper 6P-63, Proc. 25th IEEE International Conference on Plasma Science, Raleigh, NC June 1-4, 1998, ISBN 0-7803-4792-7, pp 289.

3. Corke, T. C., Jumper, E. J. Post, M. L., and McLaughlin, T. E., *"Application of Weakly-Ionized Plasmas as Wing Flow-Control Devices",* AIAA Paper 2002-0350, Proc. Of the 39th AIAA Aerospace Sciences Meeting & Exhibit, Reno NV, January 2002.

4. Cripps, S. C., *"Advanced Techniques in RF Power Amplifier Design",* Artech House Publishers, ISBN 1580532-82-9, Ch.4, June 2002.

5. Fulgosi, M., Soldati, A., and Banerjee, S., *"Turbulence Modulation by an Array of Large-Scale Streamwise Structures of EHD Origin",* Proc. Of FEDSM '99 3rd ASME/JSME Joint Fluids Engineering Conference, July 18-23 1999, San Francisco CA, pp 1-8.

6. Karakaya F., Sherman D. M., and Roth J. R. *"A Polyphase Low Frequency RF Power Supply for a One Atmosphere Uniform Glow Discharge Plasma (OAUGDP)",* Paper 3P-35, *Proc. 26th IEEE International Conference on Plasma Science*, Monterey, CA June 20-24, 1999, ISBN 0-7803-5224-6, p 178.

7. Kimura M., Tung S., Ho C., Jiang F., Tai Y. (1997) *"MEMS for Aerodynamic Control",* AIAA paper 97-2118, 28th AIAA Fluid dynamics Conference, June 29 – July 2,1997, Snowmass Village, CO.

8. Massinesm F., Ben gadri, R., Rabehi A., Decomps Ph., and Mayoux Ch., *"Experimental and Theoretical Study of a Glow Discharge at Atmospheric Pressure Controlled by Dielectric Barrier",* Journal of Applied Physics, Vol. 83, No. 6, pp 2950-2957, 1998.

9. Post, M. L., *"Phased Plasma Actuators for Unsteady Flow Control",* M.S Thesis University of Notre Dame, Indiana. July 2001.

10. Rashid, M. H., *"Power Electronics",* Prentice Hall, Inc, ISBN 0-13-678996-X, Ch.12., 1993.

11. Roth J.R. (1995). *"Industrial Plasma Engineering".* Volume 1 – Principles, Institute of Physics Publishing, Bristol and Philadelphia, ISBN 0-7503-03182, pp 453-461.

12. Roth, J. R., *"Ball Lightening: What Nature is Trying to Tell the Fusion Community"*, Proceeding of the First Symposium on Current Trends in International Fusion Research, Edited by E. Panarlla, Plenum Press, New York and London, ISBN 0-306-45513-7, pp 459-473 (1997).

13. Roth J. R. : *"Method and Apparatus for Covering Bodies with A Uniform Glow discharge Plasma and Applications Thereof"* U. S. Patent #5,669,583, Issued Sept 23, 1997.

14. Roth, J.R., *"Boundary Layer Flow Control with a One Atmosphere Uniform Glow Discharge Surface Plasma, Part I, Electrohydrodynamic Flow Control"*, AIAA paper 98-0328, 36th AIAA Aerospace Science Meeting and Exhibit, Reno NV, January 1998.

15. Roth J. R. *"Electrohydrodynamically Induced Airflow in a One Atmosphere Uniform Glow Discharge Surface Plasma"* Paper 6P-67, *Proc. 25th IEEE International Conference on Plasma Science*, Raleigh, NC June 1-4, 1998, ISBN 0-7803-4792-7, pp 291.

16. Roth, J. R. *"Neutral Gas Flow Induced by Lorentzian Collisions at Plasma Boundaries and the Possibility of Operating Fusion Reactors at One Atmosphere"* In *Current Trends in International Fusion Research-Proceedings of the 3rd Symposium* Edited by E. Panarella, NRC Research Press, National Research Council of Canada, Ottawa, ON K1A 0R6 Canada, ISBN 0-660-18480-X, (2001).

17. Roth, J. R, *"Industrial Plasma Engineering. Volume 2 , Applications to Non-Thermal Plasma Processing"*. Institute of Physics Publishing, Bristol and Philadelphia, 2002, ISBN 0-7503-0545-2, Section 18.6.

18. Roth, J. R., Sherman D. M., and Wilkinson S. P., *"Electrohydrodynamic Flow Control with a Glow Discharge Surface Plasma"*, AIAA Journal, Vol. 13, No. 7, July 2000, pp 1166-1172.

19. Roth, J. R., Tsai P. P., and Liu C., *"One Atmosphere Uniform Glow Discharge Discharge Plasma"*. U.S. Patent #5,414,324, Issued May 9, 1995.

20. Roth, J. R., Tsai P. P., *"Steady-state, Glow Discharge Plasma and Applications Thereof"*, U.S Patent #5,387,842, Issued February 7, 1995.

21. Sherman, D. M., *"Manipulating Aerodynamic Boundary Layers Using an Electrohydrodynamic Effect Generated by a One Atmosphere Uniform Glow Discharge Plasma"*, MS thesis, Department of Physics, University of Tennessee, Knoxville, August 1998.

22. Spence P. D., Liu C., Roth., *"Preliminary Measurements of the Plasma Properties of a One Atmosphere Uniform Glow Discharge Plasma"*, APS Bulletin, Vol. 38, No. 10, pp. 1901.

23. Tsinober, A. (1989), *"MHD Flow Drag Reduction"* in Viscous Drag Reduction in Boundary Layers, AIAA Progress in Astronautics and Aerodynamics, Vol. 123, Seabass A. R., ed., ISBN 0-930403-66-5, pp. 327-349.

24. Walsh M., *"Riblets, in Viscous Drag Reduction in Boundary Layers"*, AIAA Progress in Astronautics and Aeronautics, Vol. 123, Seabass A. R. ISBN 0-930403-66-5, pp 203-261.

25. Wygnanski I., *"Boundary Layer and Flow Control by Periodic Addition of Momentum"*, AIAA Paper 97-2117, 4th AIAA Shear Flow Control Conference, June 29 – July 2, Snowmass Village, CO.

VITA

Hojung Sin was born in Chungbook, South Korea on March 30, 1965 and grew up there until he came to Edmond, Oklahoma in January of 1995. He entered the University of Central Oklahoma and received a Bachelor of Science with major in chemistry and physics in December of 1998. He began his graduate study from January of 1999 at the University of Tennessee Knoxville with major in physics. He transferred to the Department of Electrical and Computer Engineering and started work as a Graduate Research Assistant at the UT Plasma Sciences Laboratory in May, 2001. The Master of Science degree is anticipated in December 2002.